Solenoidal Ionization Cooling Lattices

R.C. Fernow* and R.B. Palmer

Brookhaven National Laboratory, Upton, NY 11973

(Dated: February 21, 2007)

Abstract

We explore a practical approach for designing ionization cooling channels with periodic solenoidal focusing. We examine the lattice characteristics in terms of the properties of the coils and the cell geometry. The peak magnetic field in the coils is an important engineering constraint in lattice design. We examine the dependence of the peak field, momentum pass band locations, and the beta function on the coil parameters. We make a systematic examination of all allowed lattice configurations taking into account the symmetry properties of the current densities and the beta function. We introduce a unique nomenclature for comparing cooling lattice configurations. While solutions with a single coil per cell illustrate most of the effects that are important for cooling channel design, the introduction of additional coils allows more flexibility in selecting the lattice properties. We look at example solutions for the problem of the initial transverse cooling stage of a neutrino factory or muon collider and compare our results with the properties of some published cooling lattice designs. Scaling laws are used to compare solutions from different symmetry classes.

PACS numbers: 29.27.-a,41.85.-p

*Electronic address: fernow@bnl.gov

I. INTRODUCTION

Ionization cooling [1, 2] is an essential feature of most designs for neutrino factories [3] and muon colliders [4]. The phase space of the muon beam that comes from pion decays greatly exceeds the acceptance of downstream accelerator systems. A front end system is usually included that incorporates longitudinal phase space rotation to reduce the energy spread of the beam and cooling to reduce its transverse emittance. For the initial cooling of the muon beam the only cooling process that is fast enough compared to the muon lifetime is ionization cooling. After the beam has been cooled there is a possibility of obtaining additional cooling using the process of using optical stochastic cooling[5]. In the process of ionization cooling muons are focused onto an absorber in the beam path. The particles lose both transverse and longitudinal momentum while crossing the absorber. The beam is then passed through an rf cavity that only restores the lost longitudinal momentum. The net result is that a particle loses some of its transverse momentum and transverse cooling takes place. The cooling effect is balanced against multiple scattering, which acts to increase the emittance. The relative effect of multiple scattering is reduced if the beam is strongly focused in the absorber. Thus we see that a transverse cooling channel has three essential ingredients: an absorber, an rf cavity, and a system of some sort to focus the beam in the absorber and confine it during its transport through the cavity.

Muon colliders have the additional requirement of reducing the longitudinal emittance of the muon beam. Direct longitudinal ionization cooling using the slight relativistic rise of ionization energy loss at high energies is very inefficient. Thus the only practical method of longitudinal cooling is to use the process of emittance exchange. Dispersion is introduced into the cooling lattice, and the absorber is shaped, in such a way that reductions in longitudinal emittance are compensated by a corresponding increase in transverse emittance. Additional transverse cooling can be provided in the lattice to provide overall 6-dimensional emittance reduction. Longitudinal cooling thus introduces dispersion as one additional ingredient in the focusing lattice design. This has been accomplished in several ways for solenoid lattices. Bending a solenoid produces dispersion in the plane perpendicular to the plane of bending [6]. If a dipole field is superimposed on the bent solenoid, the transverse displacement is proportional to the deviation of the momentum from some reference value. Wedge-shaped absorbers are used to reduce the momentum spread of the dispersed beam. A design of

this type used an 8.5 m long channel [4] with the solenoid first bent in the horizontal plane to generate vertical dispersion and then bent in the vertical plane to generate horizontal dispersion.

Dispersion can also be generated in a cooling ring. The Tetra ring, which was the first design of this type [7], used dipoles for bending and solenoids for focusing. All of the focusing and bending in the RFOFO cooling ring design [8] was provided by tipped solenoids. Small cooling rings typically have a problem with injection of large emittance beams. This can be avoided by transforming the ring to a helical geometry [9], which is sometimes referred to as a "Guggenheim" configuration.

Many different types of cooling channels have been proposed. Magnetic focusing can be provided by quadrupoles, solenoids, helices or lithium lenses. The most effective application for quadrupoles seems to be as a precooler for large emittance beams [10]. Lithium lenses are most naturally used for the low emittance final stages of cooling [11]. The possible application of helices is a recent development that may have widespread applications [12]. Helices have an advantage when longitudinal cooling is required since the dispersion arises naturally. Nonetheless, most of the mature transverse cooling channel design work done so far has made use of periodic solenoid focusing. Unlike quadrupoles, solenoids have the advantage that both transverse planes are focused simultaneously.

Two types of solenoid focused channels have been studied. The first is a continuous large-aperture solenoid with rf cavities inside the coils. A uniform channel is a natural choice when a gas is used as a continuous absorber [13]. As cooling proceeds the Larmor trajectories of the particles shrink down towards the centers of their orbits. This is effectively 1-dimensional cooling since the transverse size of the beam is not affected by the cooling. Cooling of the transverse dimension can take place if field reversal sections are added to the lattice [14]. The uniform channel has the advantage that there are no restrictions on the placement of absorbers and rf cavities and that there are no stop bands in the transmitted momentum spectrum. It has the disadvantage that the large aperture magnets are expensive. In addition we will see in the next section that solenoidal cooling channels have a problem with canonical angular momentum unless part of the channel has the direction of the magnetic field reversed. This is a second reason for the necessity of adding one or more field reversal matching sections. These reversal sections tend to be complicated with the potential for emittance growth or beam loss. No channel can be continuous in practice. A

real channel must allow access for cryogenics, power leads, instrumentation or rf waveguides. Gaps must be provided between the solenoid coils to allow for this. For a given value of the beta function the uniform channel must provide a larger volume of magnetic field and it cannot easily take advantage of tapering the channel parameters as the beam cools. The alternative cooling channel for the U.S. Feasibility Study 1 [15] for a neutrino factory used a single-flip continuous solenoid channel for cooling. Another early example for the muon collider used six coils per cell in an alternating polarity lattice [4, 16, 17]. Long "continuous" solenoids surrounded the absorbers while the other coils in each cell were used for matching the beta function and gently reversing the field direction.

The second type of solenoid focused channel is a periodic lattice of solenoid magnets. One has the freedom here to place coils in optimal locations to achieve specific design goals. The use of smaller radius solenoids result in less expensive designs than the continuous solenoid channel. In addition, if the polarity of the solenoids alternate along the lattice, the canonical angular momentum problem is solved naturally. The chief disadvantage of the periodic arrays is the presence of momentum stop bands, which restrict the useable operating range.

A number of cooling lattices using periodic solenoid focusing have been designed over the past decade. Historically the first system considered had a simple sinusoidal dependence of the longitudinal field with axial position. In analogy with the common FODO channel of quadrupole lenses, this was designated a FOFO lattice [18] since each solenoid lens focuses both transverse plane simultaneously. Later, following on a suggestion by Andrew Sessler, it was found that the performance of these lattices could be improved significantly by the addition of higher harmonic terms to the on-axis fields [19]. Lattices of this type were given name "super-FOFO" or "SFOFO". By changing the coil configurations and symmetry properties a number of periodic lattice configurations were discovered. These were typically given their own unique names. One problem with this development was that the relation of these solutions to each other was not always clear. Another problem was that the chosen names were often confusing and not uniquely defined.

Some of the basic properties of a periodic solenoid lattice can be qualitatively determined with a thin lens analysis [20, 21]. A step beyond this was made by Penn [22, 23], who examined periodic solenoidal lattices in terms of the addition of second and third harmonics to the fundamental sinusoidal field. This analysis introduced a scaling variable $\chi = \frac{B_0 \lambda}{p}$

where B_0 is the peak on-axis field, λ is the period of the magnetic field and p is the momentum of the particle. Stable lattice configurations could be located on phase diagrams with χ as the abscissa and the relative amount of harmonic content as the ordinate. This type of analysis was later extended and the stable regions of the space were more clearly identified [24]. A limitation with this approach is that the magnetic field used in most of the cooling lattices adopted in practice, such as the lattice for the US Study 2 neutrino factory, have much more complex Fourier decompositions.

An alternative analysis of lattice stability and beta function symmetries has been done using recursive solutions of Hills equation [25]. This method uses Fourier coefficients of the focusing function as input. It produces power series expansions for the trace of the one-cell transport matrix as a function of momentum and for the beta function as a function of position. It was found to produce results in good agreement with the simpler method that is used in this paper.

While an analysis of lattice properties in terms of its leading harmonic content gives some important theoretical understanding of its characteristics, it is not the most practical approach for designing a cooling channel. In this paper we look instead at lattice characteristics in terms of the properties of the coils and the cell geometry. We use the number of coils in a geometric cell and the symmetry properties of the current densities and the beta function to introduce a unique nomenclature for comparing cooling lattice configurations. We separate the results presented here by the number of coils per geometric cell. We first examine solutions with a single coil per cell. This arrangement illustrates most of the effects that are important for cooling channel design. Then we examine the changes that are introduced as additional coils are added to the cell.

We show the results predicted by thin lens analysis. We examine the predictions for lattices with a perfectly sinusoidal magnetic field. This special case is important because theoretical predictions for the lattice properties can be made in terms of solutions of the Mathieu equation. This allows us to check the accuracy of our numerical techniques for calculating lattice characteristics. The peak magnetic field in the coils is an important engineering constraint in lattice design. We examine the dependence of the peak field on coil parameters. We then examine the dependence of pass band locations and beta functions on these same parameters. We develop software for optimizing lattice parameters taking the peak field constraint into account. This allows us to make a systematic examination of all

allowed lattice configurations. Finally we introduce a scaling relation to compare our results for different symmetry classes and to compare these results with the properties of some published cooling lattice designs.

II. IONIZATION COOLING LATTICES

Muon beams suffer from two major difficulties compared with normal accelerator beams. The first is due to their method of production. Pions created in the interaction of a proton beam with a target must be collected and allowed to decay into muons. The characteristics of the resulting muon beam are determined by the properties of the collection channel. Typically muon beams have a very large rms normalized transverse emittance $\epsilon_{TN} \sim 20$ mm rad and a large momentum spread. The momentum spread can be reduced to $\sim$12% rms at the expense of increased bunch length if the beam is sent through a phase rotation channel. This large emittance points out the need for transverse cooling before the beam is introduced into an accelerator chain. The second problem is the muons short lifetime (2.2 μs at rest), which demands that any cooling has to be done very quickly. The only practical method for initial cooling of muon beams is ionization cooling. Typical applications such as neutrino factories [3] require the cooled muon beam to have $\epsilon_{TN} \sim 7$ mm rad, while muon colliders [4] need $\epsilon_{TN} \sim 0.05$ mm rad.

A. Properties of cooling lattices

In ionization cooling the muon beam is focused in an absorber in the beam path. The beam loses energy by dE/dx, which reduces both the transverse and longitudinal components of the particles momentum. The absorber is followed by an rf cavity that only restores the lost longitudinal momentum. The result is a net loss of transverse momentum and a reduction in transverse emittance. The fractional change in emittance is proportional to the fractional change in momentum arising from energy loss. Multiple Coulomb scattering in the absorber material is a competing process that acts to increase the transverse emittance. The balance between the strength of these two processes determines whether net cooling takes place. If dispersion is introduced into the transport lattice and if the absorber is given a wedge shape in the transverse direction, then it is also possible to reduce the momentum

TABLE I: Values of C.

material	C [mm mrad / cm]
liquid H_2	38
liquid He	51
LiH	61
Li	69
Be	89

spread in the beam. Energy straggling in the material is the main heating term that limits the amount of longitudinal cooling.

When the competing processes of energy loss and multiple scattering become equal the beam reaches an equilibrium normalized transverse emittance given by

$$\epsilon_{TN}^{eq} \approx \frac{\beta_T E_S^2}{2\beta mc^2 L_R |\frac{dE}{dz}|} = \frac{\beta_T}{\beta} C \tag{1}$$

where β_T is the beta function from the focusing system, $E_S = 14.1$ MeV, β is the relativistic velocity factor, mc^2 is the muon rest mass, and L_R and dE/dz are the radiation length and ionization energy loss rate of the absorber material. We have collected the material-dependent properties into the quantity C. Values of C for some common materials used for ionization cooling, evaluated at the momentum for the minimum of $\frac{dE}{dx}$, are given in Table I. One wants to use absorbers where the product of radiation length and the energy loss rate is large. Hydrogen and lithium hydride are the best choices. The only other parameter that is under our control is the beta function, which we want to keep as small as possible over the length of the absorber.

Transverse ionization cooling can take place in principle at any momentum. However at low momentum the rapid rise of $\frac{dE}{dx}$ as the momentum falls leads to a blow up in the longitudinal emittance. Cooling at high momentum is uneconomical since a lot of rf power is required to replace a fixed fraction of the initial energy. For these reasons cooling channels are typically designed with a reference momentum near 200 MeV/c. The momentum is sometimes reduced in the final stages of the channel in order to reduce the value of the beta function and to take advantage of the higher value of $\frac{dE}{dx}$.

At 200 MeV/c the energy loss rate in liquid hydrogen is $\sim$0.3 MeV/cm. If the beta

function can be kept small over ∼30 cm, the total loss of energy is 9 MeV. For a 200 MHz rf cavity with a gradient of 15 MV/m and operating 30^o off the zero-crossing, we would need ∼1.2 m of cavities to replace the lost energy. Thus most of the space in a typical cell in a cooling lattice is taken up with rf cavities.

A solenoidal focusing system in a cooling channel has a large number of sometimes conflicting requirements:

- The minimum value of the beta function should be small in order to get a small equilibrium emittance.
- The beta function should remain small over an axial region longer than the absorber.
- The maximum value of the beta function should be small for reasonable transverse beam apertures.
- The momentum acceptance of the lattice should overlap the reference momentum.
- The momentum acceptance should be larger than the momentum spread of the desired beam ($\sim \pm 30\%$ full width).
- The transverse aperture must accept the transverse emittance of the beam.
- For efficient cooling the channel must have very large angular acceptance.
- Field reversals are necessary to prevent the build-up of canonical angular momentum.
- Energy straggling and transverse-longitudinal coupling should not cause loss of particles from the rf bucket.

There are also engineering constraints on any practical magnetic configuration:

- The operating current in a superconducting magnet must be smaller than the critical current corresponding to the peak field in the coil.
- The arrangement of coils must allow access to the rf cavities and absorbers.
- There may be constraints on the strength and direction of the magnetic field in the rf cavities to prevent breakdown from limiting the useful electric field gradient in the cavity.

General methods of achieving small beta functions include using a short cell length, using a phase advance near a lattice resonance, operating in one of the lower momentum pass bands, or using higher harmonics in the magnetic field.

Cooling channels differ from most other beam transport systems because they must transmit large divergence, i.e. non-paraxial, particles. In order for the rate of beam heating to be small the mean beam divergence should be much larger than the mean multiple scattering angle. In a focusing channel the beam divergence angle is given by

$$\sigma_\theta = \sqrt{\frac{\epsilon_{TN}}{\beta\gamma\beta_T}} \tag{2}$$

We substitute Eq. 1 into Eq. 2. For efficient cooling the channel needs to transmit *rms* angles at least twice as large as the equilibrium value. If the full acceptance required is 3 times the *rms* value, we find the required angular acceptance is [26]

$$A_\theta \approx 3\sqrt{\frac{2\ C}{\beta^2\gamma}}$$

For 200 MeV/c ($\beta = 0.89$, $\gamma = 2.14$) and liquid hydrogen ($C = 4.2\ 10^{-3}$) we find the required angular acceptance is $\sim$210 mrad.

Angular momentum is a complication of solenoid channels that is not encountered in other focusing systems [27]. In an empty solenoid channel with no material in the beam path the canonical angular momentum

$$\begin{aligned} L_z^c &= L_z + e\ r\ A_\phi \\ L_z^c &\approx L_z + \frac{e}{2}B_z r^2 \end{aligned} \tag{3}$$

is a conserved quantity, where L_z is the mechanical angular momentum, e is the muon charge, r is the radius of the particle, A_ϕ is the azimuthal component of the vector potential, and B_z is the solenoid field. Consider a particle far from the solenoid with no mechanical angular momentum. Then L_z^c is 0 initially. As a particle with non-zero radius crosses the radial fringe field at the entrance to the solenoid, it develops an azimuthal momentum that exactly cancels the field-dependent term in Eq. 3 and the canonical angular momentum remains 0. At the exit of the solenoid the radial fringe field is in the opposite direction, which takes away the particle's mechanical angular momentum. The situation changes however in a cooling channel where the particles lose energy in the absorbers. If we consider a case where

complete cooling has taken place and all of the particles transverse momentum is removed, the particle will travel parallel to the z axis, and the mechanical angular momentum will vanish. However, the field-dependent part of L_z^c is still present and when this particle exits the solenoid the fringe field will introduce a divergence and an emittance increase for the beam. This effect can be eliminated by placing absorbers at locations where $B_z = 0$ or by alternating the direction of the magnetic field. This can be done most naturally by using alternating polarity lattices where the field reverses in alternate cells. It can also be done by using a "continuous" solenoid channel for some distance, introducing a special field flip region, and then continuing the continuous channel with the solenoid direction reversed.

The rf cavities in cooling channels typically operate with a synchronous phase $\sim 30^o$ from the zero-crossing point of the rf wave. This provides a good deal of phase focusing, which is needed to control the energy spread coming from straggling in the absorber material. In addition the large transverse amplitude particles that are required for efficient cooling have a much different time of flight in a solenoid channel than particles that travel near the axis. Both of these effects can lead to particle losses due to particles falling out of the rf bucket. A disadvantage of operating near zero-crossing is that a greater length of rf cavities is required to replace the energy lost in the absorber.

Solenoid lattice design has traditionally been done by varying the parameters of a few coils at the boundary between lattice cells, such that beta function is preserved over a range of incident momentum values. In practice a computer program was used to minimize the beta function slopes at the cell boundary at, for example, 9 momenta spaced at 10% intervals around the central value. Although this method has been very successful in producing useful lattice designs, there is always the danger that an even better design may have been overlooked. In addition many solenoid lattice designs found this way have had unacceptably large values of the peak field in the coils. For that reason we explore a more systematic approach to solenoid lattice design in this paper. The new optimization technique places primary emphasis on obtaining a momentum pass band for the lattice at a desired reference momentum. Secondary fitting criteria include minimizing the peak field in the coil, maximizing the momentum acceptance, and minimizing the beta function at the reference momentum. Results from this analysis are presented in sections V-VII.

B. Classification of periodic solenoid lattices

One of our goals is to develop a systematic method for comparing the properties of various periodic solenoid lattices. There are several important factors that influence the lattice behavior. Every lattice has a basic geometric cell structure that is repeated many times. Cooling cells contain at a minimum an absorber to decrease the energy of the particles, an rf cavity to replace the lost energy, and magnets to provide focusing. We define the geometric cell length to be d. We assume the focusing is done with one or more solenoids in each cell. We allow the possibility that the current in these solenoids can have different polarities. We also allow that the overall polarity of the magnetic field may alternate between adjacent geometric cells. If λ is the period of the magnetic field, then we either have the case $\lambda = d$ when the magnetic field is the same in every geometric cell, or $\lambda = 2d$ when the polarity alternates. We will give prescriptions below for defining the **boundary (b)** locations between geometric cells, depending on the number of coils per cell. We define the **midpoint (m)** of a cell to be the axial position midway between the boundaries. We will see that it is useful to maintain this distinction since the lattice solutions with beta minimums at **b** and **m** can have very different behavior.

The beta function depends on the geometry of the lattice, the symmetry of the magnetic field, and on the reference momentum of the particles of interest. For cooling lattices we are mainly interested in the spatial location and size of the minimum of the beta function, since these points determine where the absorbers should be located. We will see that periodic solenoid lattices have a series of momentum pass bands. We will denote the high momentum pass band as number **1** and then count the other pass bands in order as we decrease the momentum. The spatial location of the minimum of the beta function changes for each pass band. We are primarily interested in solutions with the minimum located either at the cell boundary or at the midpoint of the cell. Solutions with multiple minima in the cell interior are also possible, but these don't appear to offer any particular advantages for cooling purposes.

In order to compare the properties of various lattice designs we need a labeling system that uniquely incorporates this lattice information. We denote cooling lattices with symbols that show the relative polarity of the coils in adjacent geometric cells, the location of the minimum of the beta function, and the number of the momentum pass band for the reference

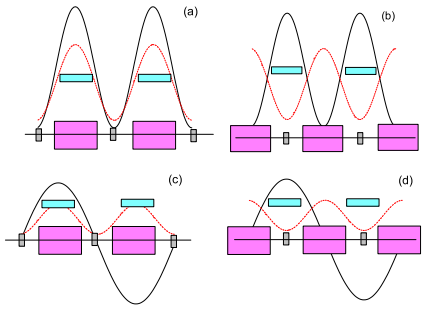

FIG. 1: (Color) The four basic lattice configurations for one coil per cell. (a) $< +|+ >$, (b)$< \hat{+}\hat{+}\hat{+} >$, (c) $< +|- >$, (d) $< \hat{-}\hat{+}\hat{-} >$.

momentum. We choose symbols that have a beta minimum in the center so that the coil arrangement on either side of the minimum is immediately apparent.

For solutions with the minimum of the beta function at the cell boundary we arbitrarily choose the first coil to have positive polarity. The boundary between the two geometric cells (defined below) is denoted with a vertical line and we append the number of the pass band as a subscript at the end of the symbol. Thus, for example, a lattice with 1 coil per geometric cell, alternating polarity in adjacent geometric cells, with the beta minimum at the cell boundary, and operation in the high energy pass band would be denoted $< +|- >_1$.

For solutions with the minimum of the beta function at the cell midplane the symbol shows the polarity of the coils in a complete cell together with the polarity of the coils up to the center of the two adjacent half-cells. We use a caret symbol to indicate the location of the minimum of the beta function. For example for a lattice with 3 coils of the same polarity per geometric cell, alternating polarity in adjacent geometric cells, with the beta minimum at the cell midplane, and operation in the second pass band, the symbol would be $< \hat{-} - +\hat{+} + -\hat{-} >_2$. For lattices with an odd number of coils per cell the minimum of the beta function would be located under one of the coils.

Figure 1 shows the four basic configurations for the case when there is one coil per cell. In these figures and in the ones that follow the rf cavities are colored magenta, the absorbers are gray, and the solenoid coils are cyan. The black solid curve is the magnetic field and the red dotted curve is the beta function.

III. SOLENOID PROPERTIES

We gather here several properties of solenoid magnets that we will require later in the paper. The focal length f of a thin solenoid lens is given by [28]

$$f = \frac{4\ p^2}{e^2 B_0^2 L}. \tag{4}$$

where p is the particle momentum, B_0 is the solenoid field strength and L is the length of the solenoid. The beta function of a uniform solenoid channel has the value

$$\beta_o = \frac{2p}{eB}. \tag{5}$$

inside the solenoid. We note that the beta function can be reduced by decreasing the operating momentum or by increasing the solenoid field strength.

For the computer calculations we use a cylindrical block description of a solenoidal coil. The coil has a total length L, inner radius a, outer radius b, and carries the current density J. If z is the axial position of an observation point measured from the center of the solenoid, then the on-axis field is given by

$$\begin{aligned} B(z) = \frac{\mu_0 J}{2}\{(L-z)\ln[\frac{b+\sqrt{b^2+(L-z)^2}}{a+\sqrt{a^2+(L-z)^2}}] \\ +(L+z)\ln[\frac{b+\sqrt{b^2+(L+z)^2}}{a+\sqrt{a^2+(L+z)^2}}]\}. \end{aligned} \tag{6}$$

This description of the solenoidal field will be used later in determining the beta functions of the lattices.

In order to investigate the peak fields in the coils we need off-axis expressions for the solenoid fields. In general both longitudinal and radial field components are present. The field component for current sheets can be expressed in closed form in terms of elliptic integrals [29]. Let us define the functions

$$b_z(r,z) = \frac{\mu_0 I'}{\pi}\frac{za}{\zeta(a+r)}[K(k) + \frac{a-r}{2a}(\Pi(k,c) - K(k))]$$

$$b_r(r,z) = \frac{\mu_0 I'}{\pi}\frac{\zeta}{4r}[2(K(k) - E(k)) - k^2 K(k))]$$

where I' is the current per unit length and we use the auxiliary quantities

$$k = \sqrt{\frac{4ar}{(a+r)^2 + z^2}}$$
$$\zeta = \sqrt{(a+r)^2 + z^2}$$
$$c = -\frac{4ar}{(a+r)^2}$$

$K(k)$, $E(k)$ and $\Pi(k, c)$ are complete elliptic integrals. The magnetic field from the solenoidal sheet is given in terms of these functions by

$$B_z(r, z) = -b_z(r, z - L) + b_z(r, z + L)$$
$$B_r(r, z) = b_r(r, z - L) - b_r(r, z + L)$$

We approximate the field of the current block by using the sum of the fields from 10 current sheets with different radii.

IV. SINUSOIDALLY-VARYING SOLENOID LATTICES

For the remainder of this paper we will consider lattices with periodically varying solenoidal fields. If we consider a particle whose energy is high enough, the period of the particles betatron oscillations Λ is longer than the geometric cell length of the lattice d. As the momentum of the particle is reduced we will eventually reach the point when $\Lambda = d$. At this point the particle sees the same radial kick at the corresponding locations in each oscillation and a resonance causes the amplitude of the motion to grow. Under these conditions the particle has a phase advance of π, so we call this the π resonance. If the momentum continues to be reduced we will reach the condition that the particle makes two betatron oscillations while traversing each cell of the lattice and a second (2π) resonance occurs. In general resonances occur whenever $\lambda = nd$, where n is an integer.

A. Mathieu analysis

Stable solutions for the motion of charged particles in lattices with sinusoidally varying magnetic fields can be found from the eigenvalues of the Mathieu equation [30–33]. The radial and azimuthal equations of motion of a charged particle are given in cylindrical

coordinates as

$$\ddot{r} - r\dot{\phi}^2 = \frac{er\dot{\phi}B_z}{m\gamma}$$
$$\frac{m\gamma}{r}\left(r^2\ddot{\phi} + 2r\dot{r}\dot{\phi}\right) = -q\dot{r}B_z$$

where the dots are time derivatives and we neglect any changes in γ. If we assume that the azimuthal acceleration can be neglected, the azimuthal equation reduces to

$$\dot{\phi} = -\frac{qB_z}{2m\gamma}$$

Requiring this constraint decouples the radial and azimuthal motions. This is known as the Larmor frame of reference. In a constant solenoid field in the laboratory frame the Larmor frame rotates with a constant angular velocity. In the case here with a periodically reversing field the Larmor frame oscillates back and forth. The radial equation becomes

$$\ddot{r} + \frac{r}{4}\left(\frac{eB_z}{m\gamma}\right)^2 = 0$$

If we now assume that near the axis

$$B_z(z) = B_0 \sin(kz)$$

we find the radial equation

$$\ddot{r} + r\left(\frac{eB_0}{2m\gamma}\right)^2 \sin^2(kz) = 0$$

This equation can be transformed into the canonical form of the Mathieu equation

$$\frac{d^2y}{d\nu^2} + (a - 2q\cos(2\nu))\ \ y = 0$$

The parameter

$$q = \left(\frac{eB_0\lambda}{8\pi p}\right)^2$$

where λ is the period of the magnetic field and p is the momentum of the particle. For the case considered here the parameter $a = 2q$. Stable, periodic solutions of the Mathieu equation only exist for certain values of the parameter q.

The first five stop bands for particle momentum in a sinusoidally varying solenoid field are given in Table II. We will use these results in the following section to check the accuracy of our computer calculations of the lattice properties.

TABLE II: Mathieu stop bands.

Stop band	$q(low)$	$q(high)$
1	0.3290	0.8898
2	1.8582	3.0391
3	4.6270	6.4259
4	8.6316	11.0480
5	13.8711	16.9047

B. Symplectic integrator method

We can examine the properties of finite size, i.e. non-thin lens, coils by evaluating the one-cell transport matrix numerically using a second order symplectic integration algorithm [34]. We break the cell up into a large number of parts, each part consisting of a half-step of drift, a thin lens and another half-step of drift. The focusing strength K of the thin lens is determined from the local value of the on-axis solenoid field from

$$K(z) = \left(\frac{eB_z(z)}{2\,p} \right)^2$$

The accuracy of this method is very good as we demonstrate below in comparisons of the tracking results with the predictions of the Mathieu theory for lattices with sinusoidal magnetic fields.

Note that the focusing strength is proportional to B^2. Unlike quadrupoles, solenoids focus the beam regardless of the direction of the field. There are however differences in angular beam dynamics since reversing the field causes the particles to rotate in opposite directions, or equivalently it reverses the direction of the angular momentum. These differences affect the radial dynamics only if transverse fields are introduced, e.g. to obtain dispersion.

C. Peak field

Purely sinusoidal field lattices have a severe problem with peak fields in large-radius solenoid coils [35]. An exact solution of the field using Maxwells equations in cylindrical

coordinates can be written as

$$B_z(r,z) = A\cos\left(\frac{2\pi z}{\lambda}\right) I_0\left(\frac{2\pi r}{\lambda}\right)$$
$$B_r(r,z) = A\sin\left(\frac{2\pi z}{\lambda}\right) I_1\left(\frac{2\pi r}{\lambda}\right)$$

where I_0 and I_1 are modified Bessel functions. For example, at a radius equal to the cell length (half the period of the magnetic field λ) the value of the function I_0 is 5.5, the value of the function I_1 is 4.5, and the peak field is $\sim$7 times the desired field value A on the axis.

V. LATTICES WITH ONE SOLENOID PER CELL

We now consider cooling lattices with one solenoid coil in each geometric cell. The four characteristic designs of this type were illustrated in Fig. 1. There are five continuous parameters and one symmetry factor that determine the properties of these lattices $\{d, L, a, t, J; f_e\}$, where L is the length of the coil, a is the inner radius, t is the radial thickness and J is the current density. The outer radius of the coil is $b = a + t$. We will use the **external symmetry parameter** (f_e) to indicate whether the polarity of the current in the coils alternate in neighboring geometric cells. We use f_e = -1 if the polarity flips and f_e = +1 if the polarity remains the same. Solutions must obviously satisfy the constraint $L < d$. We define the cell boundary (b) to be the axial location midway between the coils and the cell midplane (m) to be the axial position through the center of the coil.

A. Thin lens approximation

Let us start by examining the lattice using the thin lens approximation. This analysis is applicable to the solutions with minimums of the beta function at the cell boundary. Consider the case where we begin the matrix calculation in the center of one of the solenoids. Then the one-cell transport matrix M is the product

$$M = F\left(\frac{f}{2}\right) D(d) F\left(\frac{f}{2}\right)$$

where F is the 2x2 matrix for a thin lens of focal length $f/2$ and D is the matrix for a drift space of length d. This matrix is then compared to the standard form of the Courant-Snyder

matrix

$$\begin{vmatrix} \cos\psi + \alpha\sin\psi & \beta\sin\psi \\ -\gamma\sin\psi & \cos\psi - \alpha\sin\psi \end{vmatrix}$$

This allows us to immediately determine the relations for the phase advance per cell and the maximum value of the beta function

$$\cos\psi = 1 - \frac{d}{2f}$$
$$\beta_{max} = \frac{d}{\sin\psi}$$

The minimum value of β_{max} occurs when the phase advance is $\pi/2$. The scale of the magnitude of the beta function is set by the cell length d. We can find an expression for the minimum value of the beta function by calculating a new matrix beginning midway between the solenoids

$$M = D\left(\frac{d}{2}\right) F(f) D\left(\frac{d}{2}\right)$$

This gives

$$\beta_{min} = \frac{d}{2\sin\psi}\left(1 + \cos\psi\right)$$

If we now use the expression for the focal length of the a thin solenoid lens from Eq. 4, we find that the phase advance per cell is given by

$$\cos\psi = 1 - \frac{e^2 B_0^2 L d}{8p^2} \tag{7}$$

For very high momentum particles the phase advance is $\sim$0. As p decreases the phase advance reaches a maximum value of π when

$$p_\pi = \frac{eB_0}{4}\sqrt{Ld} \tag{8}$$

Below this momentum Eq. 7 for the phase advance becomes unphysical and there is a stop band in the momentum spectrum. The minimum value of the beta function approaches 0 at the edge of the stop band. This type of analysis fails when real solenoids have lengths that are a significant fraction of the cell length d.

B. Peak field enhancement

The range of allowed coil parameters is strongly constrained by the field enhancement on the solenoid coil. The peak field on the coil usually occurs near the inner surface. In the

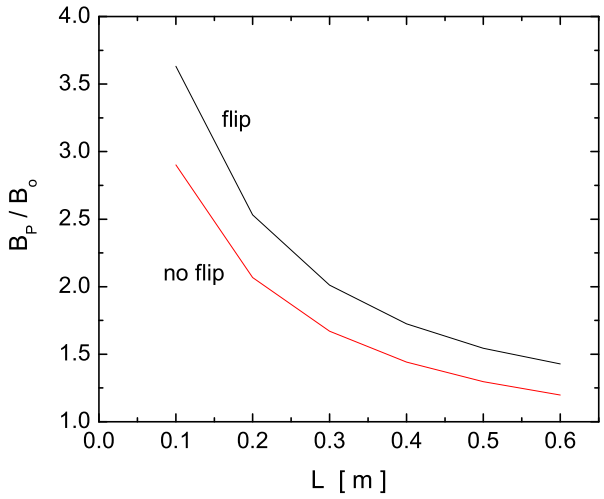

FIG. 2: (Color) Peak field enhancement as a function of the length of the coil. The other parameter values were $d = 100$ cm, $a = 40$ cm, $t = 10$ cm, and $J = 100$ A/mm^2.

design work here we try to keep the engineering current density at or below 100 A/mm^2 at 4.2 K. This limits the peak field to ∼8 T for NbTi coils and ∼17 T for Nb_3Sn coils [36]. In addition there are stress limitations that constrain the coil parameters [37]. A rule of thumb in solenoid design is that the criterion

$$\sigma_p[MPa] = B_z[T]\ r[m]\ J[\frac{A}{mm^2}]\ <\ 350$$

should be satisfied for all locations in the coil, where σ_p is the peak stress, B_z is the field in the coil at the radius r, and J is the current density. If this criterion is violated it is likely that the conductor will not be able to support the magnetic stresses without the addition of high-strength non-conducting support layers.

The peak field decreases with increasing cell length for the no-flip case if the coil dimensions remain the same. The peak field for both cases increases with the length of the coil. Figure 2 shows the dependence of the peak field enhancement on the length of the coil. The peak field enhancement decreases as the coil is made longer if the other dimensions remain the same. The enhancement is larger when the polarity flips in alternate cells. The peak field for both cases decreases with increasing radius of the coil. The peak field for a given radius is smaller for the case where the polarity flips in alternate cells.

The central field and the peak field in the coil grow linearly with the current density. For

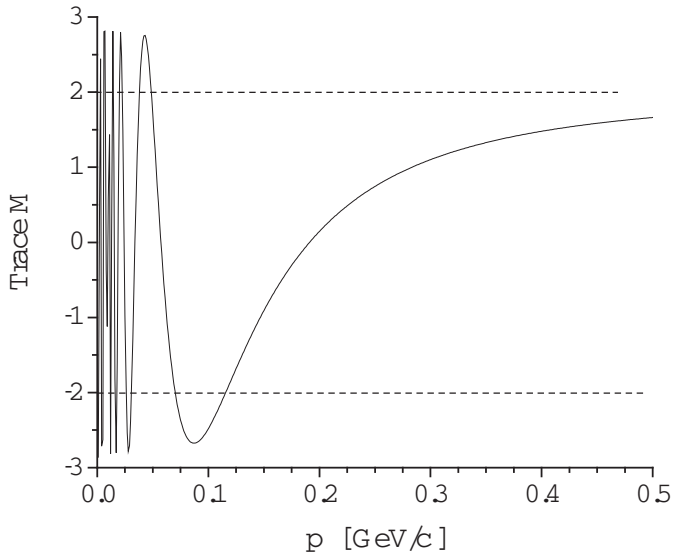

FIG. 3: Trace of the one-cell transport matrix versus momentum. The parameter values were $d =$ 100 cm, $L = 67.1$ cm, $a = 43.6$ cm,$t = 12.6$ cm, $J = 40$ A/mm^2 and alternating polarity.

a given current density the central and peak fields are larger for the no-flip case. The central field and the peak field in the coil also grow approximately linearly for coil thicknesses for the parameter range considered here. For a given radial thickness the central and peak fields are larger for the no-flip case.

C. Sinusoidal field approximation

In order to compare the results of our lattice calculations using the symplectic integrator with the Mathieu theory we first found the single coil configuration that gave the best approximation to a pure sine field on-axis. The results from an optimization program produced a very pure sine wave field. The stability of a solution can be found from the trace of the one-cell transport matrix. Solutions are stable provided the absolute value of the trace is less than 2. Figure 3 shows a plot of the trace versus momentum for the sine wave solution. We see that as predicted by the thin lens theory the lattice transmits high momentum particles. As the momentum drops we reach the upper edge of the π resonance at 116 MeV/c, whereas the thin lens prediction from Eq. 8 is 173 MeV/c. However, Fig. 3 also shows additional momentum pass bands below 70 MeV/c, which were not present in the thin lens theory.

The momentum pass band structure from this coil configuration are quantitatively com-

TABLE III: Momentum passband locations [MeV/c].

q	one-coil passband	Mathieu theory
0.329-0	116-∞	116-∞
1.86-0.890	49-70	49-70
4.63-3.04	31-37	31-38
8.63-6.42	23-26	23-26
13.87-11.05	18-19	18-20

pared with the Mathieu theory results in Table III. The momentum values for Mathieu theory come from the relation

$$p = \frac{eB_0\lambda}{8\pi\sqrt{q_M}} \tag{9}$$

where $B_0 = 2.78$ T, $\lambda = 2$ m and the q_M values for the pass bands are taken from Table II. The agreement with theory is excellent. The high energy pass band has $< +|- >_1$ symmetry while the second band has $< \hat{-}\hat{+}\hat{-} >_2$ symmetry. Each of the additional lower momentum bands has an additional minimum of the beta function in the interior of the cell.

D. Lattice properties

The minimum and maximum values of the beta function are shown as a function of p in Fig. 4. At the edge of every stop band the minimum value of the beta function in the cell approaches 0, while the maximum value of the beta function becomes very large. This general behavior of the beta function as a function of momentum does not depend on the polarity of the magnetic field in alternate cells. In some lattices the axial position where the beta minimum occurs in a given pass band changes as the momentum is varied. We define the lower edge of the high energy pass band to be p_π. We are also interested in the possibility of using the second pass band for cooling. The beta function is flatter and the maximum value of β_{min} is limited in this pass band. We define p_2 to be the center of this pass band and Δp_2 to the full width of the band. The dashed line in the figure shows the linear dependance of the beta function on momentum for a continuous solenoid expected from Eq. 5. Note how the minimum and maximum beta functions in each pass band approach the value for the continuous solenoid.

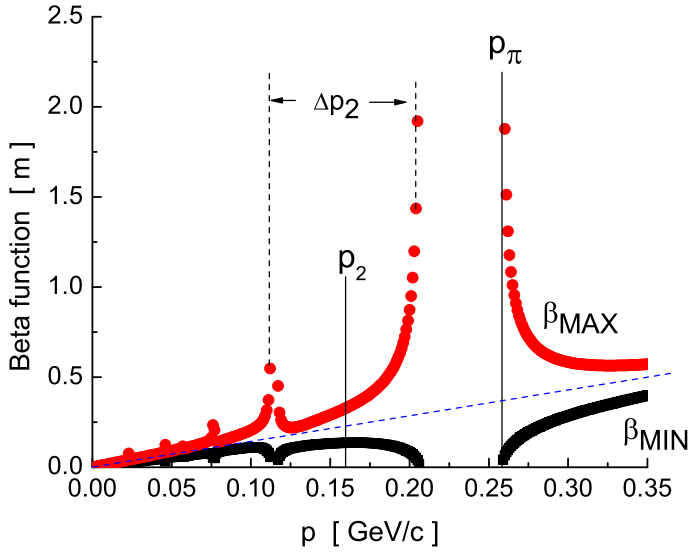

FIG. 4: (Color) Minimum and maximum values of the beta function as a function of p. The parameter values were d = 100 cm, L = 40 cm, a = 40 cm, t = 10 cm, J = 100 A/mm^2 and constant polarity.

1. Location of the momentum pass bands

The momentum of the π resonance increases with the length of the cell if the coil dimensions remain fixed. The dependence is stronger for the alternating polarity case. The center of the second pass band increases for alternating polarity, but is insensitive to cell length for constant polarity.

Figure 5 shows the momentum dependence as a function of the coil length L. The length of the solenoid has a strong effect on the value of p_π, and on the location and width of the second, lower momentum pass band for constant polarity. As L/d increases the second pass band moves up in momentum and expands in acceptance. At $L/d = 0.9$ the one-cell transport matrix at the low momentum edge of the second pass band just reaches a trace of 2 and the stop bands below this have disappeared. In the limit when $L/d = 1$ we have a continuous solenoid and there are no resonances or stop bands. The effect of changing L is somewhat weaker for alternating polarity. The location of p_π and p_2 grows at first, but then saturates for the limit L/d=1. The width of the second pass band Δp_2 never becomes

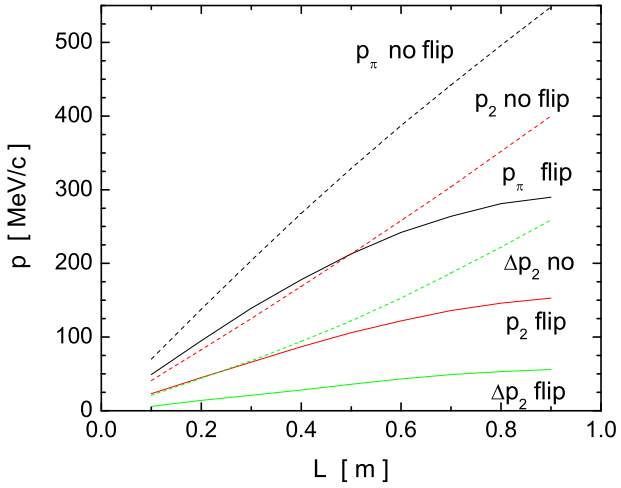

FIG. 5: (Color) Location of the π resonance, and the midpoint and width of the second band as a function of L. The other parameter values were $d = 100$ cm, $a = 40$ cm, $t = 10$ cm, and $J = 100$ A/mm^2.

very large.

We next consider changes in the pass bands as we vary the radius of the coil. Figure 6 shows the location of the π resonance, and the midpoint and width of the second band as a function of the coil radius. Increasing the radius decreases the location of the π resonance, especially in the flip case. It also decreases the midpoint of the second band for the flip case. Note however that p_2 is independent of radius for the no-flip case. The width of the second band is largest for large radius coils in the no-flip case.

The location of the π resonance, and the midpoint and width of the second band grow linearly with the current density. These quantities also grow approximately linearly with coil thickness.

The location of the π resonance can be estimated for alternating polarity lattices from the Mathieu theory. Since $q_M = 0.329$ at p_π and $q_M \approx 1.375$ at p_2, we can use Eq. 9 to find that

$$p_\pi = 20.8\ B_0\lambda \qquad (10)$$
$$p_2 = 10.2\ B_0\lambda$$

where the units are {MeV/c, T, m}. This expression should become more accurate as

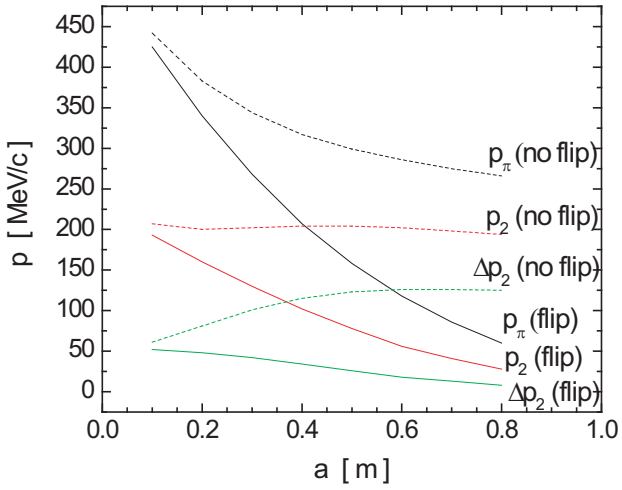

FIG. 6: (Color) Location of the π resonance, and the midpoint and width of the second band as a function of the coil radius. The other parameter values were $d = 100$ cm, $L = 50$ cm, $t = 10$ cm, and $J = 100$ A/mm^2.

the field in the lattice approximates a pure sine wave. We have found that p_2 only scales approximately with B_0 and that Δp_2 does not scale with B_0 at all. B_0 and p_π have similar dependences on the coil parameters. For very non-sinusoidal fields, e.g. lattices with small a/d and L/d and constant polarity, p_π is still approximately linearly related to B_o, but not to $B_o d$.

2. Beta function

For the high energy pass band the minimum value of the beta function is determined mainly by the separation of the reference momentum from p_π. This can be seen in Fig. 7. This figure shows the beta functions for two different coil configurations designed to have p_π at 100 MeV/c. One solution (A1) is a no-flip case, while the other solution (A2) is a flip case. We will discuss the properties of these solutions later in section V E. It is possible to reduce the beta function by moving the reference momentum closer to p_π, but this reduces the momentum acceptance.

We turn now to the minimum value of the beta function evaluated at the center (p_2) of the second pass band. We examine the dependence of the solutions on the geometrical parameters under the constraint that p_2 is fixed. Figure 8 shows the value of the beta

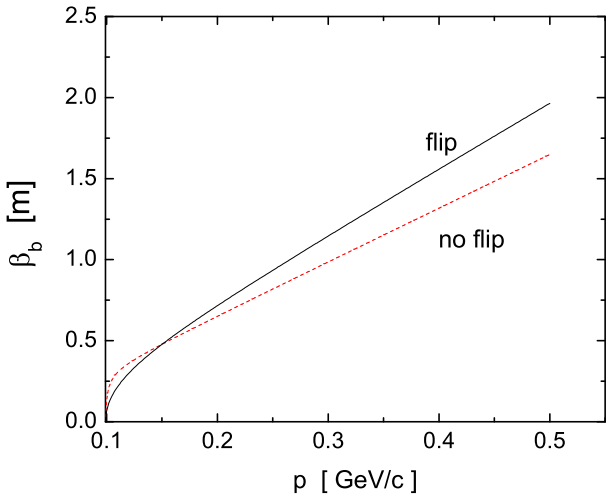

FIG. 7: (Color) Minimum beta function in the high energy pass band versus momentum. The minimum value occurs at the cell boundary.

function at the cell boundary and cell midplane and the momentum acceptance of the band as we vary the cell length for the no flip case. The other coil dimensions were kept constant. We adjusted the current density in the coils in order to keep p_2 fixed at 200 MeV/c. Note that as the cell length is increased the beta function at the cell boundary increases, but the value of the beta bunction at the midplane and the momentum acceptance both decrease. The beta function is always smaller at the midplane than at the cell boundary. Similar behavior can be seen for the flip case in Figure 9. Again we see that as the cell length is increased the beta function at the cell boundary increases, but the value of the beta bunction at the midplane and the momentum acceptance both fall. The beta function is much smaller at the midplane than at the cell boundary.

There is little dependence of the lattice parameters on the coil length if we require p_2 to be fixed. The peak field decreases slightly for longer coils. In the limit when L/d=1 the value of the beta function for the no-flip case agrees with Eq. 5 for the continuous solenoid. We show the dependence of the lattice parameters on the inner radius of the coil in Figure 10 for the no flip case. Note that the momentum acceptance can be increased by increasing a, although the beta function under the coil also increases.

In the case when p_2 is kept fixed, the values of the beta function at the boundary and

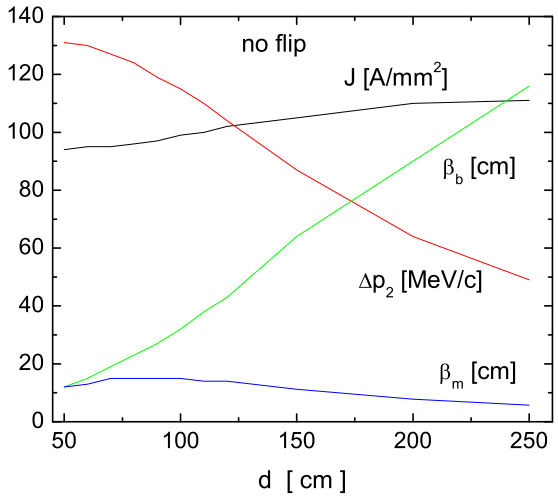

FIG. 8: (Color) Value of the beta function at the cell boundary and midplane, momentum acceptance, and current density to keep p_2 fixed at 200 MeV/c for the no flip case. The other parameter values were $L = 20$ cm, $a = 40$ cm, and $t = 24$ cm.

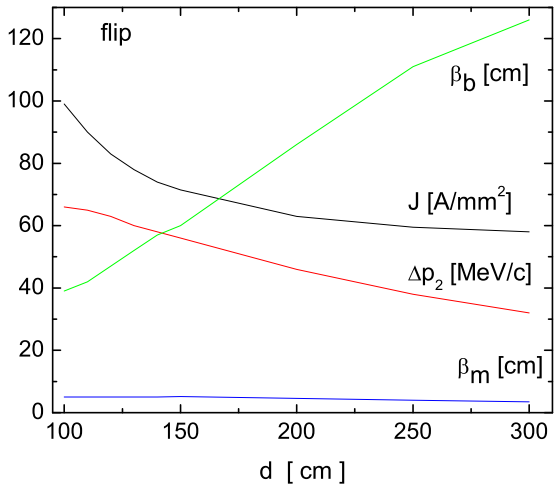

FIG. 9: (Color) Value of the beta function at the cell boundary and midplane, momentum acceptance, and current density to keep p_2 fixed at 200 MeV/c for the flip case. The other parameter values were $L = 40$ cm, $a = 35$ cm, and $t = 24$ cm.

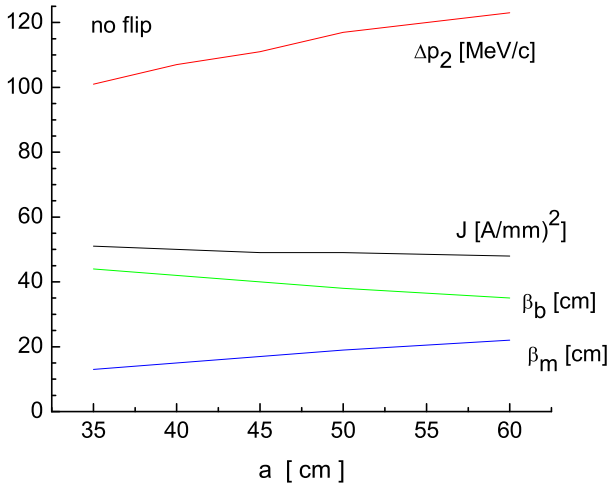

FIG. 10: (Color) Value of the beta function at the cell boundary and midplane, momentum acceptance, peak field, and current density to keep p_2 fixed at 200 MeV/c for the no flip case. The other parameter values were $d = 120$ cm, $L = 40$ cm, and $t = 24$ cm.

midplane are insensitive to changes in the coil thickness. As the current density and the resulting magnetic field is varied, the location of the second pass bands changes, as we saw in the previous section, but the minimum value of the beta function in the center of the pass band remains constant.

For the cases considered here the minimum value of the beta function at the center of the pass band is proportional to the width of the band. For a given coil length the no-flip configuration generates much wider pass bands than the flip configuration. In general it is difficult to find solutions that have both a low beta function and a wide momentum acceptance.

E. Representative lattices

In order to examine specific examples of the various classes of possible lattices we need to select a particular cooling objective. We will look for solutions that would be suitable for the early stages of a neutrino factory or muon collider. With just a single coil per cell we will take $d = 1 - 2$ m. A typical reference momentum is 200 MeV/c. We will try to provide a momentum acceptance of ± 100 MeV/c. The beam radius is typically 30 cm, so we set a

lower limit on a of 35 cm. Examples of this type of channel use rf cavities with frequency around 200 MHz, which has a radius ∼60 cm. We take the length of the cavity to be at least 50 cm. We can satisfy these conditions either by using short coils of small radius located between cavities, or by using longer coils with large radius located around the rf cavity. For solutions with the minimum value of the beta function at the cell boundary (b) the natural arrangement is to use a large radius coil surrounding the rf cavity. For solutions with the minimum value of the beta function at the midplane (m) of the cell the natural arrangement is to use a short, small radius coil over the absorber.

We first look at solutions that use the high energy pass band. All momenta greater than p_π are transmitted by the lattice. We see from Fig. 7 that the minimum beta function increases steadily as the momentum increases. Since we want a reference momentum (p_0) around 200 MeV/c and a momentum acceptance ±100 MeV/c, our primary fitting criterion is to find solutions with $p_\pi = 100$ MeV/c. Solution **A1** uses large radius coils that could fit outside the rf cavities and that have constant polarity. This is an example of an $< +|+ >_1$ lattice. Both the minimum values of the beta function and the magnetic field occurs at the boundaries of the cell. The beta function is very flat with a minimum value of 65 cm and a maximum value of 67 cm. Solution **A2** also uses large radius coils, but has alternating polarity. It is an example of an $< +|- >_1$ lattice. Both the minimum values of the beta function and the magnetic field occurs at the boundaries of the cell. The minimum value of the beta function is 72 cm and the maximum value is 87 cm.

Next we consider solutions which make use of the second pass band. These solutions produce much smaller values of the beta function than those in the first pass band. For the same application described earlier our primary fitting criterion now is to find solutions with the center of the band around 200 MeV/c. Ideally we would like the total width of the band to also be ∼200 MeV/c, so the accepted momentum range would be 100-300 MeV/c, but this has not been achieved in practice.

Solution **A3** has a constant polarity lattice and is an example of a $< \hat{+}\hat{+}\hat{+} >_2$ lattice. Since the field does not change polarity we would eventually have to stop this lattice when the canonical angular momentum builds up. A polarity-reversing matching section would need to be provided and then the same type of lattice could be continued with the opposite sign of the field. The minimum value of the beta function, which is 16 cm, occurs in the middle of the cell. The beta function rises to 80 cm at the cell boundaries. Solution **A4**

TABLE IV: Summary of the one-cell lattice solutions

	sine	A1	A2	A3	A4	Study 2a
type	$<+\|->_1$	$<+\|+>_1$	$<+\|->_1$	$<\hat{+}\hat{+}\hat{+}>_2$	$<\hat{-}\hat{+}\hat{-}>_2$	$<+\|->_1$
d [cm]	100	100	100	200	200	75
L [cm]	67.1	30	40	74	80	15
a [cm]	43.6	70	70	50	50	35
t [cm]	12.6	6	14	25	35	15
J [A/mm^2]	40	90	91	27	26	107
p_π [MeV/c]	116	100	100	380	431	85
p_2 [MeV/c]	60	71	50	200	201	41
Δp_2 [MeV/c]	21	45	17	87	64	13
p_0 [MeV/c]	200	200	200	200	200	220
$\beta_{abs}(p_0)$ [cm]	58	65	72	16	9	73
B_0 [T]	2.8	2.1	2.4	4.7	5.5	2.8
B_p [T]	4.1	4.3	7.9	6.0	7.1	7.5

has an alternating polarity lattice and is an example of a $<\hat{-}\hat{+}\hat{-}>_2$ configuration. The minimum value of the beta function, which is 9 cm, occurs in the middle of the cell. The beta function rises to 75 cm at the cell boundaries.

Typical parameters are shown in Table IV together with results for the other one-cell lattice configurations. The quantity β_{abs} is the beta function at the absorber location, which can be either at the boundary or the midplane depending on the solution.

F. Example: Study 2a cooling channel

A single coil per cell design was used for the cooling channel in U.S. Study 2a for a neutrino factory [38]. A layout of the channel is shown in Fig. 11. The rf cavity is colored magenta, the absorbers are gray and the coils are cyan. The configuration of this lattice differs from the canonical forms shown in Fig. 1. It was designed to have a very flat beta function, as shown in Fig. 12. This meant that there was little penalty in not locating the absorbers at the minimum of the beta function. It was convenient to make the absorbers

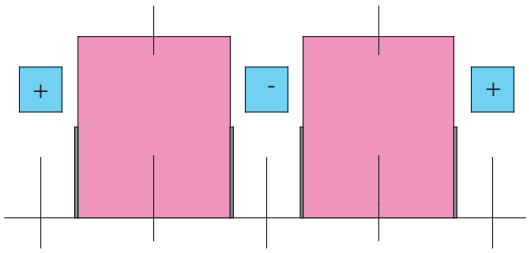

FIG. 11: (Color) Layout of the Study 2a cooling channel. The cell boundaries are in the centers of the rf cavities.

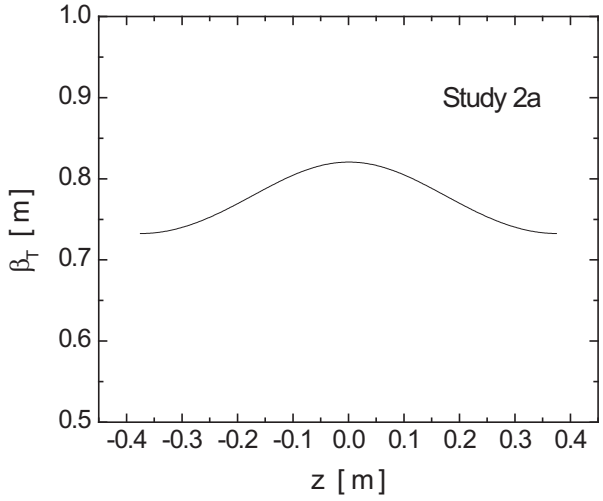

FIG. 12: Beta function for the Study 2a cooling lattice as a function of z.

part of the window assembly for the pillbox type rf cavity. For the reference momentum the minimum beta function was 73 cm, while the beta function at the absorber was 80 cm. The dependence of the beta function on momentum is shown in Fig. 13. The minimum and maximum values of the beta function along the cell are shown as solid lines. The squares indicate the beta function at the cell boundary. Note that the cell boundary coincides with the minimum of the beta function for all momenta in the high energy pass band used by Study 2a. The Fourier sine series composition of the magnetic field is dominated by the first order term with a small 4.6% contibution from the third order. Other properties are listed in Table 3. For this and other examples from the literature in the following sections, the fields and lattice parameters are the results of the calculations described here and sometimes differ slightly from the results presented in the original papers.

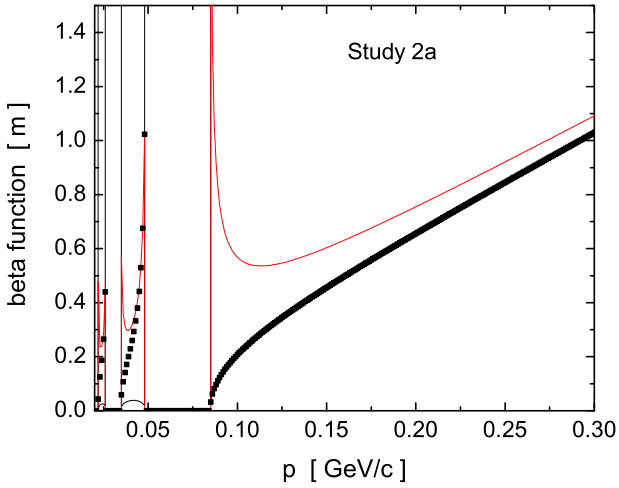

FIG. 13: (Color) Beta function for the Study 2a cooling lattice as a function of p.

VI. LATTICES WITH TWO SOLENOIDS PER CELL

We now consider cooling lattices with two solenoid coils in each geometric cell. In the most general case the two coils could be totally different and this would introduce many more parameters than were available with one coil per cell. However, we will restrict our consideration to cases where the two coils have the same length and radii and have the same magnitudes of current density. In this case we allow an additional **internal symmetry factor** f_i that specifies whether the two coils internal to the unit cell have the same (f_i=1) or opposite (f_i=-1) polarity. There is also one additional continuous parameter g that specifies the gap separation of the coils from their nearest symmetric neighbor coil across the cell boundary, as shown in Fig. 14. Thus in this section we will examine the properties of lattices based on the eight parameters in the set $\{d, L, a, t, J, g; f_e, f_i\}$. Solutions must satisfy the constraint $g + 2L < d$.

In order to uniquely specify the distance g we start by picking any coil **C**. Call the distance from **C** to the nearest coil on the left d_L and the distance from **C** to the nearest coil on the right d_R. Then we define the **gap (g)** as $g = min\{d_L, d_R\}$. The maximum value of the gap is then $g_{max} = d/2 - L$. We define the cell boundary (b) to be the axial location that bisects the gap, i.e. b is at g/2. We define the cell midplane (m) to be the axial position midway between the cell boundaries. In the case of equally spaced coils where $d_L = d_R$ there is an

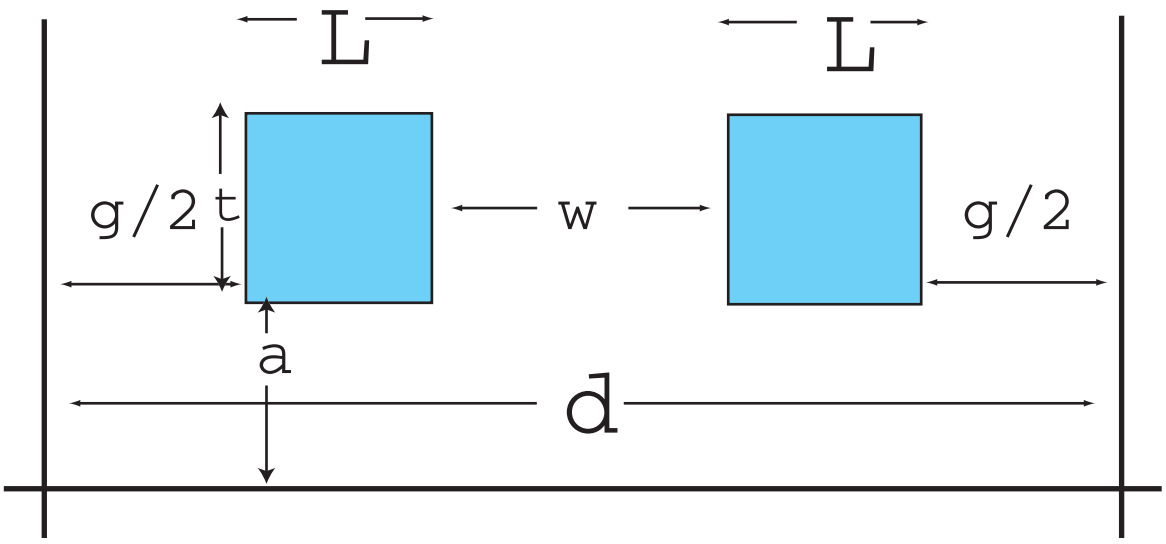

FIG. 14: (Color) Geometric properties of the two-coil unit cell.

ambiguity in the definition of the lattice notation. For example the sequence of coils + + – – + + could be denoted either by $< ++ | -- >$ or by $< +- | -+ >$. However, both of these lattice classes produce the same result in this limit. This special case does not reduce to a lattice with one coil per geometric cell.

Having two coils per cell allows more flexibility in cooling lattice design. As we discuss below it is often possible to change the momentum acceptance in the second pass band by varying g. This also changes the location of the pass band, but J can then be adjusted to recenter the band.

A. Thin lens matrix analysis

Consider first the thin lens analysis of the two-coil cell. If we break the cell down to

$$M = D\left(\frac{g}{2}\right) F(f) D(d-g) F(f) D\left(\frac{g}{2}\right)$$

we find that the phase advance per cell is given by

$$\cos\psi = 1 - \frac{d}{f} + \frac{gd}{2f^2} - \frac{g^2}{2f^2} \tag{11}$$

Note the quadratic dependence of the phase advance on the distance g. The minimum value of the beta function is

$$\beta_{min} = \frac{1}{\sin\psi}\left(d - \frac{gd}{f} + \frac{g^2}{2f} + \frac{g^2 d}{4f^2} - \frac{g^3}{4f^2}\right)$$

If we instead break the cell down as

$$M = F\left(\frac{f}{2}\right) D(d-g)F(f)D(g)F\left(\frac{f}{2}\right)$$

we find the maximum value of the beta function is

$$\beta_{max} = \frac{1}{\sin\psi}\left(d - \frac{gd}{f} + \frac{g^2}{f}\right)$$

B. Peak field

The peak field in the coil increases for all symmetry classes for increasing L, t, and J when the other dimensions are held constant. The peak field decreases for increasing a. For changes in d the peak field increases when f_i=-1 and decreases when f_i=+1. The peak field for all cases goes up as g is decreased, which corresponds to the case where the two neighbor coils across the cell boundary come close together.

C. Lattice properties

In general a rich variety of behavior is seen in the two-coil configuration making it more difficult to specify simple rules for predicting the lattice properties. The location of the π resonance increases for all symmetry classes for increasing L, t, and J when the other dimensions are held constant, while it decreases for increasing a. For changes in d the location of the π resonance increases when f_i=-1 and is approximately constant when f_i=+1. The dependence on d is particularly strong for the $< + - | - + >$ symmetry class.

The dependence of the π resonance on the distance g is shown in Fig. 15. Varying the gap between the coils across the boundary has little effect on the locations of the π resonance for the symmetry classes with $f_e = +1$, but it has a very strong effect for the other two classes. Note the degenerate behavior of the $< + + | - - >$ and $< + - | - + >$ symmetry classes at g_{max}.

We now look at the behavior of the properties of the second pass band under the constraint that p_2 is fixed at 200 MeV/c. Fig. 16 shows the width of the pass band, and the beta functions at the cell boundary and at the cell midplane as a function of g for the $< ++|-- >$ symmetry class. We also show the value of the current density required to keep p_2 constant. The distance g can be used to adjust the momentum acceptance of the band. As g decreases

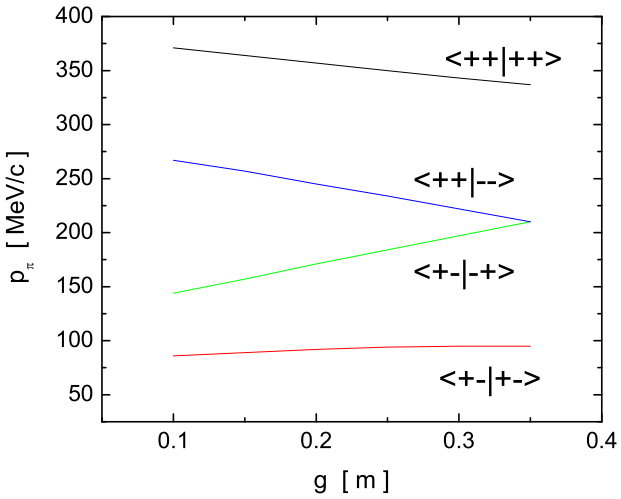
400
350
300
250
200
150
100
50
0.1
0.2
0.3
0.4
p_π [MeV/c]
g [m]
<++|++>
<++|-->
<+-|-+>
<+-|+->

FIG. 15: (Color) Location of π resonance as a function of g. The other parameter values were $d =$ 150 cm, $L = 40$ cm, $a = 50$ cm, $t = 10$ cm, and $J = 70$ A/mm^2.

the beta function at the boundary also decreases, while the beta function at the midplane increases. Note that β_b is smaller than β_m here, unlike the case for one coil per cell. The effects of varying g on the momentum aceptance can be seen more clearly in Fig. 17. For small g the acceptance is symmetric around p_2. For larger g the acceptance increases. However, as the value of g approaches g_{max} the focusing becomes too weak, the acceptance becomes distorted, and the beta function becomes very large at the upper end of the band. This distortion also occurs when a is made large.

D. Representative lattices

We have used the example initial cooling problem from the previous section to search for representative two-coil solutions. We try to find small radius solutions with the coils located between the rf cavities. For solutions with the minimum value of the beta function at the cell boundary we would locate the rf cavity at the cell midplane, whereas for solutions with the minimum of the beta function at the midpoint of the cell we would locate the rf cavity across the cell boundary between adjacent cells.

A summary of characteristic solutions for the high energy pass band is given in Table V. All of the B solutions in Table V have a cell length of 1.5 m and a reference momentum of

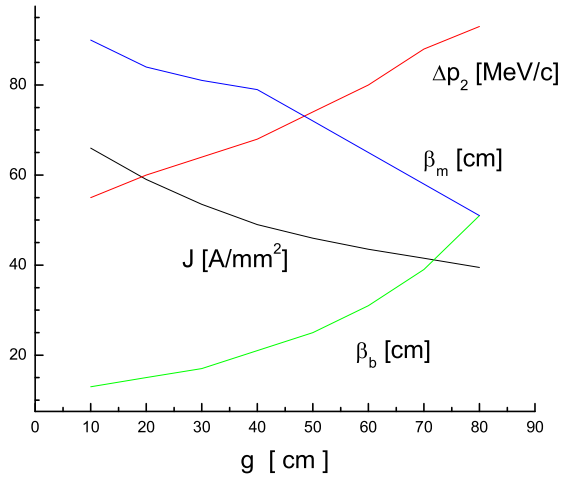

FIG. 16: (Color) Width of the second pass band, peak field, and beta function at the cell boundary and cell midplane as a function of g for the $< + + | - - >$ symmetry class. The other parameter values were $d = 275$ cm, $L = 50$ cm, $a = 35$ cm, and $t = 11$ cm.

200 MeV/c. They all have the π resonance located around 100 MeV/c, so the half-width of the momentum acceptance is also 100 MeV/c. Note that solutions for a given pass band and given coil current density polarities can have different beta function symmetries. Most of these solutions, other than **B3**, have the wrong natural symmetry for optimal cooling. Nevertheless in the table we assume the absorber is located at the cell boundary, which is the center of the intercell gap. The quantity β_{abs} is the beta function at the absorber. In most cases this is not the minimum value of the beta function in the cell. The quantity L_{rf} is the larger intercoil spacing in the cell, which is centered on the cell midplane. The **B3** solution appears best for cooling purposes. It has a beta function at the absorber location of 94 cm at the reference momentum. There is an 80 cm gap available for locating the rf cavity. The peak field in the coil is less than 5 T.

A summary of characteristic solutions for the second momentum pass band is given in Table VI. All of the B solutions in Table VI use a cell length of 2 m and a reference momentum of 200 MeV/c. Each of them has the center of the second pass band located around 200 MeV/c. Three of these B solutions have the beta minimum at the cell boundary, which is the correct natural symmetry for optimal cooling. These solutions have smaller beta functions at the absorber and less momentum acceptance than the solutions in Table V. Solution **B6**

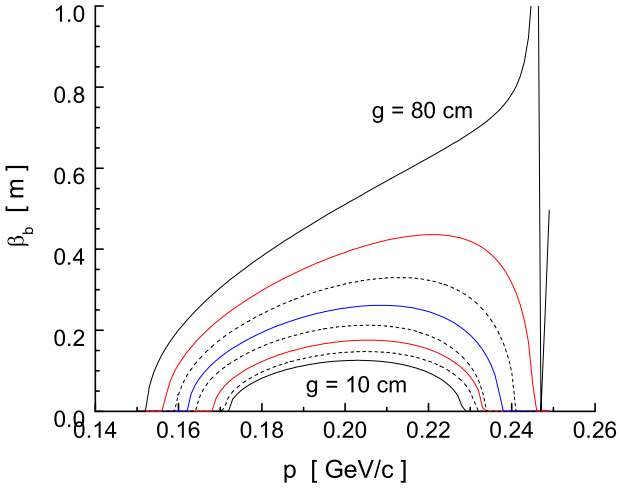

FIG. 17: (Color) Beta function at the cell boundary as a function of p for the $< ++|-- >$ symmetry class. The value of g starts at 10 cm, then increases in increments of 10 cm. The other parameter values were $d = 275$ cm, $L = 50$ cm, $a = 35$ cm, and $t = 11$ cm.

would be suitable for cooling, provided that occasional field-flip matching sections are added. The **B8** solution appears best for cooling purposes. It has a beta function at the absorber location of 13 cm at the reference momentum, although the full momentum acceptance is only 74 MeV/c. There is a 79 cm space available for locating the rf cavity. The peak field in the coil is 5.5 T. The **B9** example shows that two-coil solutions also exist for the second pass band with the minimum of the beta function at the cell midplane.

E. Example cooling channels

We consider two examples from the literature that use two coils per geometric cell. Both of these examples differs from the characteristic solutions examined in the previous section by having a large radius. The first example is the baseline cooling lattice from the U.S. Feasibility Study I for a neutrino factory [15, 39]. A layout of the channel is shown in Fig. 18. Both Nb_3Sn coils in each cell have the same polarity. This is a $< ++|-- >_1$ configuration. The beta function along the cell is shown in Fig. 19. The minimum value of the beta function is 42 cm. The momentum acceptance is smaller than the examples in Table V. The cell boundary coincides with the minimum of the beta function for all momenta

TABLE V: Summary of the two-cell high-energy pass band characteristic solutions.

	B1	B2	B3	B4	B5	Study 1
type	[a]	[b]	[c]	[d]	[e]	[c]
d [cm]	150	150	150	150	150	110
L [cm]	20	25	20	20	20	30
a [cm]	37	35	37	37	36	68
t [cm]	5	10	10	10	6	35
J [A/mm^2]	66	77	81	92	79	49
g [cm]	20	15	30	20	45	30
p_π [MeV/c]	101	100	101	100	100	156
p_2 [MeV/c]	54	66	79	74	60	80
$\beta_{abs}(p_0)$ [cm]	124	112	94	100	118	42
L_{rf} [cm]	90	85	80	90	65	80
B_0 [T]	1.6	1.9	1.9	1.9	1.6	3.4
B_p [T]	2.7	5.0	4.8	5.7	3.4	9.4

[a] $<++\hat{}++>_1$
[b] $<-+\hat{}-+>_1$
[c] $<++|-->_1$
[d] $<-+\hat{}+->_1$
[e] $<++\hat{}-->_1$

in the high energy pass band used by Study 1. The Fourier harmonics are dominated by the fundamental mode with only a 0.6% contribution from the third order term. Other properties of the channel are shown in Table V. The peak field in the conductor is satisfactory for Nb_3Sn coils.

The second example is the transverse cooling lattice that was used as the basis for the RFOFO cooling ring [8]. A layout of the channel is shown in Fig. 20. The two coils in each cell have opposite polarity. This is a $<+-|+->_2$ configuration. The beta function along the cell is shown in Fig. 21. The minimum value of the beta function is 40 cm. The dependence of the beta function on momentum is shown in Fig. 22. The minimum and maximum values of the beta function along the cell are shown as solid lines. The squares indicate the beta function at the cell boundary. Note that the cell boundary coincides with

TABLE VI: Summary of the two-cell characteristic solutions for the second momentum pass band.

	B6	B7	B8	B9	RFOFO
type	[a]	[b]	[c]	[d]	[b]
d [cm]	200	200	200	200	275
L [cm]	34	47	47	46	50
a [cm]	40	40	40	40	77
t [cm]	16	20	16	20	11
J [A/mm^2]	42	47	40.5	36.8	95.3
g [cm]	44	27	27	40	60
p_π [MeV/c]	314	275	364	278	264
p_2 [MeV/c]	200	199	201	200	198
Δp_2 [MeV/c]	97	84	74	97	88
$\beta_{abs}(p_0)$ [cm]	24	24	13	30	40
L_{rf} [cm]	82	79	79	68	215
B_0 [T]	3.6	3.9	4.1	3.6	2.7
B_p [T]	5.3	6.5	5.5	5.4	7.4

[a] $<++|++>_2$
[b] $<+-|+->_2$
[c] $<+-|-+>_2$
[d] $<-\hat{}+-+->_2$

the minimum of the beta function for all momenta in the second energy pass band used by the RFOFO design. The RFOFO field is predominantly a double sine wave with a 10% contribution of fourth harmonic and a 1.8% contribution of sixth harmonic. Other properties of the channel are shown in Table VI.

VII. LATTICES WITH THREE SOLENOIDS PER CELL

We next consider cooling lattices with three solenoid coils in each geometric cell. In the most general case the three coils could be totally different and this would introduce many more parameters than were available with two coils per cell. However, a simpler

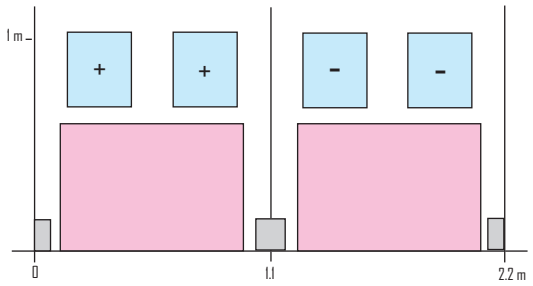

FIG. 18: (Color) Layout of the Study 1 cooling channel.

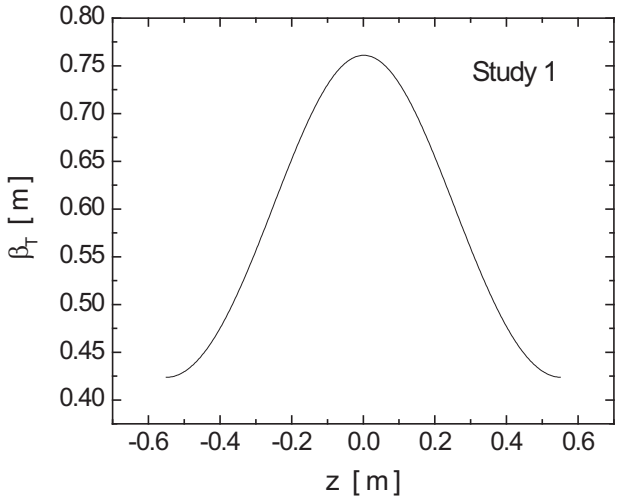

FIG. 19: Beta function for the Study 1 cooling lattice.

way to make use of the new coil is to use the current in the third coil as a means of adjusting the lattice properties without modifying the geometry. Thus we will restrict our consideration to symmetric cases where the two outer coils have the same length, radii and current density. We will denote these as the *focusing* coils. We assume the third coil, which we call the *coupling* coil, is located symmetrically between the focusing coils. We will place

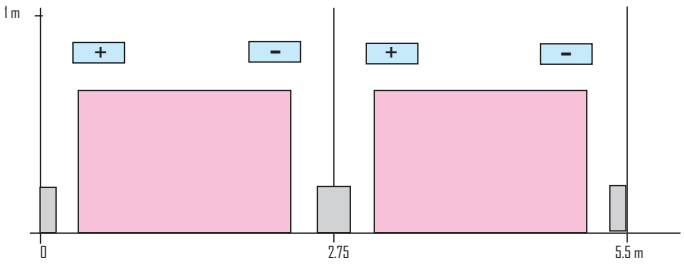

FIG. 20: (Color) Layout of the RFOFO cooling channel.

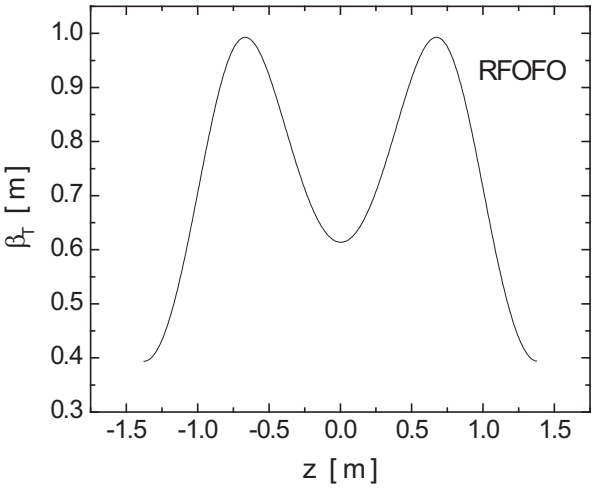

FIG. 21: Beta function for the RFOFO cooling lattice.

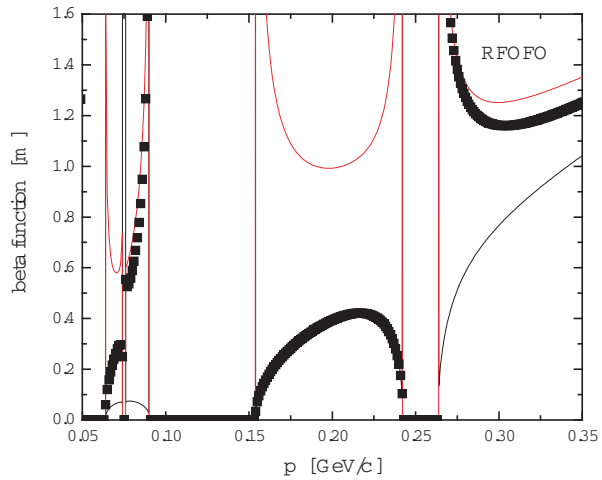

FIG. 22: (Color) Beta function for the RFOFO cooling lattice as a function of p.

no restrictions on the length, radii or current density of the coupling coil. The relative polarity of the current density between the focusing and coupling coils will be specified using an internal symmetry factor f_i. As before we use f_e to indicate whether the overall polarity flips (f_e= -1) or not (f_e= 1) in alternate cells. The layout of the geometric cell is shown in Fig. 23.

The gap g is the distance between the rightside focus coil in one geometric cell and the leftside focus coil in the next geometric cell. There is one additional axial parameter h that specifies the length of the coupling coil. Thus in this section we will examine the properties

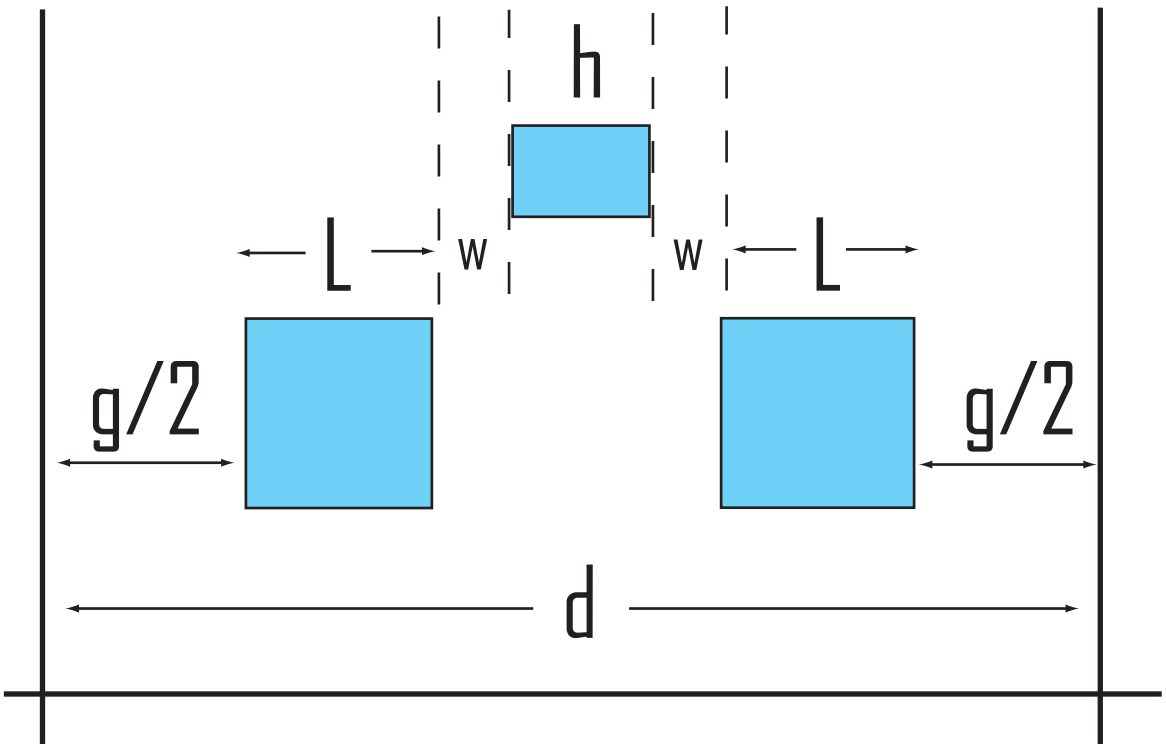

FIG. 23: (Color) Axial layout of the unit cell with three coils per cell.

of lattices based on the 12 parameters in the set $\{d, L, a, t, J, g, h, a_c, t_c, J_c; f_e, f_i\}$. Solutions must satisfy the constraint $2L + g + h < d$. We define the cell boundary (b) to be the axial location that bisects the gap, i.e. b is at g/2. We define the cell midplane (m) to be the axial position midway between cell boundaries, i.e. m is at the center of the coupling coil. There is no ambiguity in the definition of the cell boundary in the case of equally spaced coils with the same dimensions and the same magnitude of the current density since we are requiring both focusing coils to have the same polarity.

Having two adjustable currents in each cell gives us a "tunable" lattice for the second pass band. One can use the coupling coil J_c to set the momentum acceptance and beta function at the absorber. Then the band can be recenterd at the desired momentum by adjusting the focusing J. In this way the properties of the lattice can be adjusted without changing the size or location of the coils. For example the beta function can be tapered to follow the reduction in beam emittance from cooling.

The thin lens analysis for this case contains many additional terms containing the focal length of the coupling coil and is not particularly enlightening. The peak field in these configurations can occur in either the focusing or the coupling coil. In terms of the new

variables the peak field is not very sensitive to changes in g or a_c. The peak field does however grow approximately linearly with h for all the symmetry classes. In general the peak fields for 200 MeV/c reference momentum solutions are smaller with three coils per cell than the corresponding solutions with one coil per cell.

A. Lattice properties

With the large number of available parameters it is difficult to make completely general statements about the properties of the three-coil lattice configurations. The location of the π resonance can be changed by varying the gap distance g or the coupling coil length h. The π resonance increases in momentum for increasing h for all symmetry classes when the coupling coil is long.

The direct relationship between the minimum value of the boundary beta function at p_2 and the width of the second pass band is also seen for the case of three coils per cell. The dependence of some properties of the second pass band on the coupling coil length for the $< + + +| - - - >$ symmetry class are shown in Fig. 24. The location and width of the band increase with increasing h. The minimum value of the beta function occurs at the cell boundary for h up to ∼30 cm for this example and then switches to the cell midplane for longer coils. This shows that the character of the solution can be changed by varying the length of the coupling coil. The dependence of some properties of the second pass band on the current density in the coupling coil for the $< + + +| - - - >$ symmetry class is shown in Fig. 25. For this figure the current density in the focusing coils was adjusted to keep p_2 fixed at 200 MeV/c. The width of the band tends to grow for increasing coupling current. The minimum value of the beta function occurs at the cell boundary for h up to ∼95 A/mm^2 for this example and then switches to the cell midplane for higher current densities. This shows that the character of the solution can also be changed by varying the relative currents in the coupling and focus coils.

B. Representative lattices

We have used the example initial cooling problem from the previous sections to search for representative three-coil solutions. We try to find solutions where either the focusing

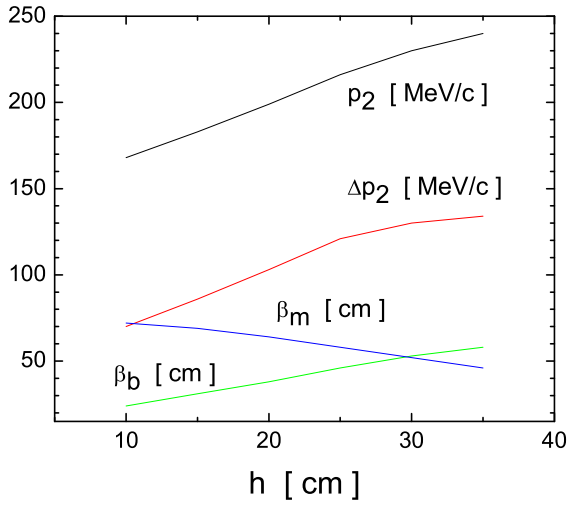

FIG. 24: (Color) Location of the center of the second pass band p_2, the width of the band, the beta function at the cell boundary β_b and the beta function at the cell midplane β_m as a function of the distance h. The other parameter values were $d = 2.5$ m, $L = 18$ cm, $a = 35$ cm, $t = 17$ cm, $J = 73$ A/mm^2, $g = 54$ cm, $a_c = 70$ cm, $t_c = 12$ cm, and $J_c = 75$ A/mm^2.

coils or the coupling coil have small radius and are located between rf cavities. The other coil then has to have a large radius and be located outside the rf cavity. The most desirable solution with small focusing coil radius has the minimum of the beta function at the cell boundary, while solutions with small coupling coil radius want the minimum to occur at the cel midplane.

A summary of characteristic solutions for the high energy pass band is given in Table VII. The maximum length available for the rf cavity is $d-g-2L$ for solutions with small focusing coil radius and $d-h$ for soultions with small coupling coil radius. None of these solutions offer any obvious advantage over lattices with one or two coils per cell.

A summary of characteristic solutions for the second pass band is given in Table VIII. Solution **C8** is an attractive solution for early cooling. It is an $<+++|---->_2$ configuration with a minimum beta funtion of 38 cm and a band width of 103 MeV/c.

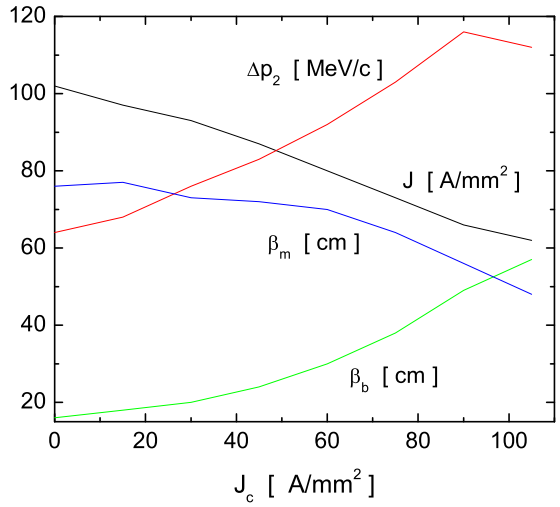

FIG. 25: (Color) The current density J in the focusing coils, the width of the second pass band, the beta function at the cell boundary β_b and the beta function at the cell midplane β_m as a function of the current density J_c in the coupling coil. The other parameter values were $d = 2.5$ m, $L = 18$ cm, $a = 35$ cm, $t = 17$ cm, $g = 54$ cm, $h = 20$ cm, $a_c = 70$ cm, and $t_c = 12$ cm.

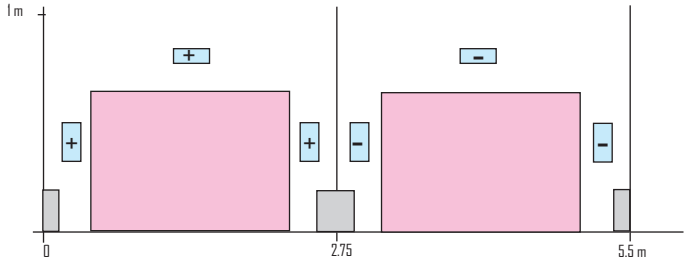

FIG. 26: (Color) Layout of the Study 2 cooling channel.

C. Example: Study 2 cooling channel

The cooling lattice from the second U.S. feasibility study for a neutrino factory [3, 40, 41] uses three coils per cell. A layout of the channel is shown in Fig. 26. All three coils in each cell have the same polarity. The beta function along the cell is shown in Fig. 27. The minimum value of the beta function is 49 cm. This is an $<+++|--->_2$ configuration. The dependence of the beta function on momentum is shown in Fig. 28. The minimum and maximum values of the beta function along the cell are shown as solid lines. The squares

TABLE VII: Summary of the three-cell characteristic solutions for the first pass band. All of these solutions have $d = 2$ m.

	C1	C2	C3	C4
type	[a]	[b]	[c]	[d]
L [cm]	10	25	16	30
a [cm]	40	75	39	76
t [cm]	5	5	6	8
J [A/mm^2]	69	50	70	46
g [cm]	50	50	38	30
h [cm]	30	67	30	65
a_c [cm]	70	35	70	35
t_c [cm]	5	5	6	5
J_c [A/mm^2]	63	50	65	49
p_π [MeV/c]	99	100	101	101
p_2 [MeV/c]	73	41	66	35
$\beta_{abs}(p_0)$ [cm]	129	152	130	154
L_{rf} [cm]	130	133	130	135
B_0 [T]	1.1	1.5	1.1	1.5
B_p [T]	2.4	2.0	2.9	2.6

[a] $<+++|+++>_1$
[b] $<+-+|+-+>_1$
[c] $<+++|---->_1$
[d] $<+-+|-+->_1$

indicate the beta function at the cell boundary. Note that the cell boundary coincides with the minimum of the beta function for all momenta in the second energy pass band used by the Study 2 design. The Fourier decomposition of the magnetic field contains very strong contributions from the odd higher order harmonics. The amplitude of the third order term is 41% and the amplitude of the fifth order term is 34% of the fundamental. Other properties of the channel are shown in Table VIII.

TABLE VIII: Summary of the three-cell characteristic solutions for the second pass band.

	C5	C6	C7	C8	C9	Study 2
type	[a]	[b]	[c]	[d]	[e]	[d]
d [cm]	250	250	250	250	250	275
L [cm]	30	15	30	18	30	16.7
a [cm]	75	35	75	35	35	33
t [cm]	10	25	10	17	14	17.5
J [A/mm^2]	49	72	49	73	70	75.2
g [cm]	30	88	30	54	70	35
h [cm]	80	42	80	20	20	33
a_c [cm]	35	74	35	70	70	77
t_c [cm]	10	5	14	12	10	8
J_c [A/mm^2]	56	-70	55	75	65	98
p_π [MeV/c]	486	320	538	274	293	274
p_2 [MeV/c]	201	199	199	199	201	194
Δp_2 [MeV/c]	52	69	36	103	70	117
$\beta_{abs}(p_0)$ [cm]	7	19	4	38	22	49
L_{rf} [cm]	170	132	170	160	120	205
B_0 [T]	5.3	3.5	6.2	3.1	3.6	2.8
B_p [T]	6.0	7.1	7.2	6.4	6.5	6.4

[a] $<\hat{-}-+\hat{+}+-\hat{-}>_2$
[b] $<+-+|+-+>_2$
[c] $<\hat{-}+-\hat{+}-+\hat{-}>_2$
[d] $<+++|---->_2$
[e] $<+-+|-+->_2$

VIII. SCALING RELATIONS

Any of the lattice solutions discussed in the the previous sections can be scaled geometrically to produce additional lattices that may be more satisfactory for other conditions. Suppose we scale all the cell dimensions by the same factor f. Then it follows from Eq. 7 that we can obtain the same on-axis field by scaling the current density by $1/f$. However,

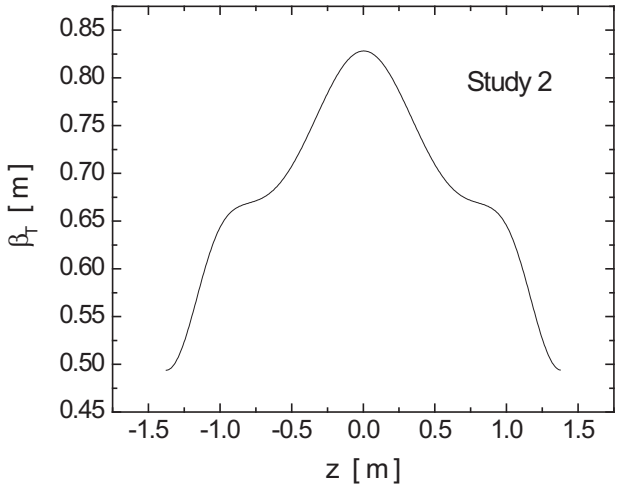

FIG. 27: Beta function for the Study 2 cooling lattice.

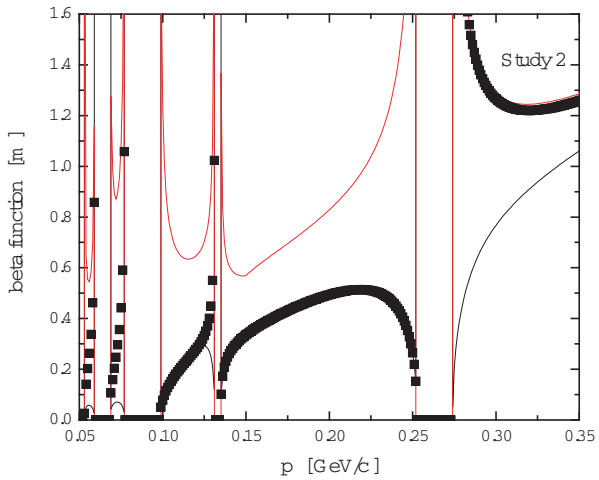

FIG. 28: (Color) Beta function for the Study 2 cooling lattice as a function of p.

we have seen in Eq. 11 that the pass band locations scale like $B_o d$. Thus we need to scale the current density like $1/f^2$ to keep the pass band locations fixed. This is illustrated in Fig. 29 where the scale factor of 1 corresponds to the **A4** example. The current density was adjusted to keep p_2 fixed at 200 MeV/c. The peak field in the coil falls with increasing scale factor. The maximum on-axis field is proportional to the peak field in the coil. Both the beta function at the boundary and at the midplane grow linearly with increasing scale factor. However, note that the magnitude of the beta function at the midplane is still quite small ($\sim$ 13 cm for a 3 m cell length). The momentum acceptance (not shown) is independent of

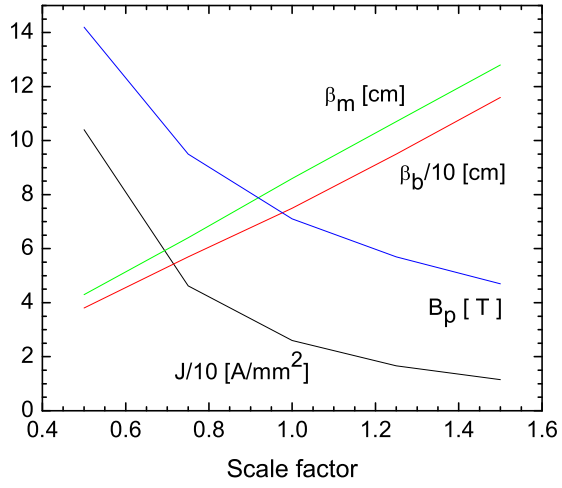

FIG. 29: (Color) Geometrical scaling of the **A4** example lattice.

the scale factor.

In the previous sections we have systematically examined the characteristics of cooling lattices with increasing number of coils per cell. In order to compare solutions with different numbers of coils per cell and different symmetry classes it is useful to introduce another scaling variable. We have seen that there is often a direct relationship between the magnitude of the beta function and the momentum acceptance. Since the beta function depends on the scaling parameter f, we can define a normalized beta function corresponding to a fixed maximum axial field. We then examine how this scaled beta function depends on the momentum acceptance.

We define the scaled momentum acceptance as

$$\delta = \pm\frac{p - p_\pi}{p} \text{ for the first pass band}$$
$$\delta = \pm\frac{\Delta p_2}{2p_2} \text{ for the second pass band}$$

We define the scaled beta function F_1 as the actual beta function for some lattice normalized to the value of the beta function for the continuous solenoid evaluated with the same value of the maximum on-axis field. Using Eq. 5

$$F_1 = \frac{\beta}{\beta_o} = \beta\frac{eB_o}{2p}$$

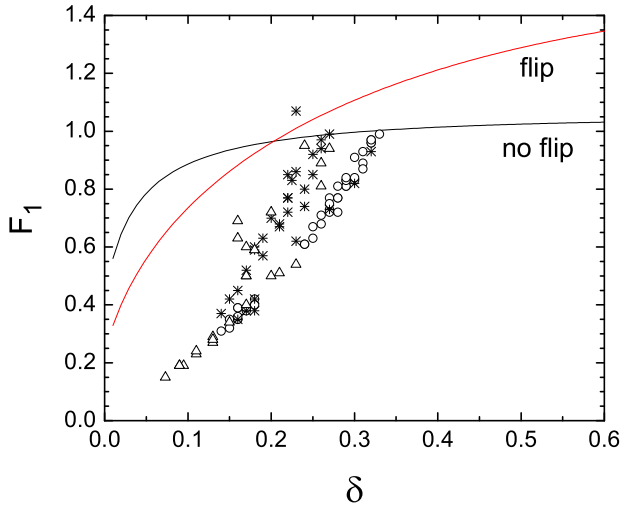

FIG. 30: (Color) Scaled beta function as a function of scaled acceptance. The solid lines show first pass band results for the flip (A2) and no flip (A1) example lattices. Symbols show second pass band solutions with $p_2 = 200$ MeV/c; ∘: 1 coil per cell, ∗: 2 coils per cell, △: 3 coils per cell.

The scaled behavior of some of the example lattices discussed previously are shown in Fig. 30. Large regions of the first pass band solutions and most of the second pass band solutions have F_1 smaller than 1 and thus produce more efficient cooling than a continuous solenoid. In the first pass band alternating-polarity lattices are more advantageous for small momentum acceptance. At the beginning of cooling the momentum spread of the beam is large. In this case one would use a lattice operating in the first pass band because any value of the momentum acceptance is possible in principle by operating far enough away from p_π. However, the beta functions for these lattices are also large. After a sufficient amount of longitudinal cooling reduces the momentum spread to $\sim \pm 30\%$ full width one can switch to a lattice that uses the second pass band and has smaller beta functions at the absorbers. The scaled behavior of some of the example lattices discussed previously are shown in Fig. 31. For each of these example solutions the radius was changed to vary the momentum acceptance and the current density was adjusted to recenter the band at 200 MeV/c. The direct relationship between the minimum beta function and the momentum acceptance can be clearly seen in this figure.

One can proceed through a number of these stages, leading finally to a lattice with small

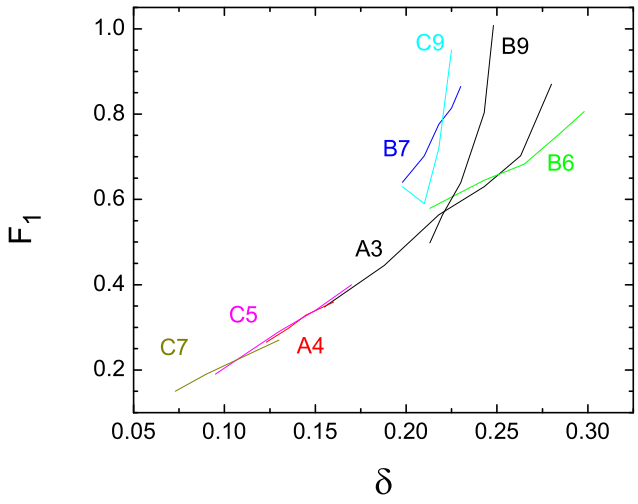

FIG. 31: (Color) Scaled beta function as a function of scaled acceptance for example lattices for the second pass band centered at 200 MeV/c.

acceptance and very small beta function. For $\delta \geq 10\%$, using current 25 T HTS technology, the smallest beta function using solenoid focusing appears to be ∼1 cm.

IX. SUMMARY

Ionization cooling channels play an important role in the design of neutrino factories and muon colliders. In this paper we have summarized the status of cooling lattice design using periodic solenoid focusing. There is considerable flexibility in the design of these channels and they exhibit a great variety of interesting properties. The detailed behavior of the lattice properties is strongly influenced by the symmetries exhibited by the polarities of the currents in the coils in the periodic channel. In order to describe this behavior we introduced a new system for classifying the symmetry properties of periodic solenoid cooling lattices. A method using symplectic integration of the one-cell transport matrix was used to calculate momentum stop bands and beta functions. This integration used the on-axis field calculated from solenoid coil blocks. We found this method was accurate by showing that a sinusoidally-varying magnetic field gave results in good agreement with predictions from solutions of the Mathieu equation. The peak field in the coil was an important design

constraint. We showed how the peak field in the coil and the lattice properties depend on the geometric properties of the coils.

We introduced a new optimization procedure that emphasizes obtaining a desired momentum band and minimizing the peak field in the coil. We used this method to systematically search for lattice configurations that could be used in a neutrino factory or muon collider. We saw that most features of the lattice dynamics could be seen even in the simplest case of a single coil per geometric cell. There are two momentum pass bands that have been used for cooling lattices. The beta function in the high momentum band is determined mainly by the amount of momentum acceptance that is required. The location of the π resonance scales with the maximum value of the on-axis magnetic field. The minimum value of the beta function and the momentum acceptance are typically much smaller in the second pass band. The momentum acceptance can be adjusted by varying the radius and length of the coil.

Adding a second coil per geometric cell adds considerable flexibility for cooling channel design. The gap between the two coils across the cell boundary is an important design parameter that can have strong effects on the momentum acceptance and other lattice properties. In addition the number of possible symmetry classes is doubled. With three coils per cell it is possible to design a "tunable" lattice with fixed coil positions and radii. The focusing coil current is used to set the acceptance and the beta function value at the absorber, while the coupling coil current is used to center the location of the pass band. The properties of different lattice types were compared using a scaled value of the beta function. The value of the beta function is directly related to the momentum acceptance. For all the coil configurations we have produced sample solutions for each of the symmetry classes. Several of these lattice designs have interesting properties and might be suitable for further investigation for the transverse cooling channel of a neutrino factory or muon collider.

Acknowledgments

We would like to thank G. Penn, J.S. Berg and V. Balbekov for useful discussions on some of the topics covered in this paper. This effort was supported by the Office of High

Energy Physics of the U.S. Department of Energy under contract DE-AC02-98CH10886.

---

[1] A.N. Skrinsky and V.V. Parkhomchuk, Sov. J. Part. Nucl. **12**, 223 (1981).

[2] D. Neuffer, Part. Accel. **14**, 75 (1983).

[3] M. M. Alsharo´a *et al.*, Phys. Rev. ST Accel. Beams **6**, 081001 (2003).

[4] C.M. Ankenbrandt *et al.*, Phys. Rev. ST Accel. Beams **2**, 081001 (1999).

[5] A.A. Mikhailichenko and M.S. Zolotorev, Phys. Rev. Lett. **71**, 4146 (1993).

[6] J. C. Gallardo et al., in *Physics Potential and Development of $\mu\mu$ colliders*, edited by D. Cline (1998), vol. 441, pp. 282–288.

[7] V. I. Balbekov et al., in *Proceedings of the 2001 Particle Accelerator Conference* (2001), pp. 3867–3869.

[8] R. Palmer *et al.*, Phys. Rev. ST Accel. Beams **8**, 061003 (2005).

[9] A. Klier, `http://mice.iit.edu/nfmcc06/nfmcc06_klier_guggenheimchannel.pdf`.

[10] C. Johnstone *et al.*, Nucl. Instrum. & Meth. **A519**, 472 (2004).

[11] V. Balbekov, in *Proceedings of the 1999 Particle Accelerator Conference* (1999), pp. 3146–3148.

[12] Y. Derbenev and R.P. Johnson, Phys. Rev. ST Accel. Beams **8**, 041002 (2005).

[13] R.B. Palmer, `http://www.fnal.gov/projects/muon_collider/eexchange/workshop03/palmer1.pdf`.

[14] V. I. Balbekov et al., in *Proceedings of the 2001 Particle Accelerator Conference* (2001), pp. 3870–3872.

[15] N. Holtkamp and D. Finley, eds., Tech. Rep. Fermilab-Pub-00/108-E, Fermilab (2000), `http://www.fnal.gov/projects/muon_collider/nu-factory/nu-factory.html`.

[16] R. Palmer, in *Physics Potential and Development of $\mu\mu$ colliders*, edited by D. Cline (1998), vol. 441, pp. 183–208.

[17] R. C. Fernow, in *Advanced Accelerator Concepts*, edited by W. Lawson et al. (1998), vol. 472, pp. 233–242.

[18] R. Palmer *et al.*, Nucl. Phys. B (Proc. Suppl.) **51A**, 61 (1996).

[19] E.-S. Kim *et al.*, Tech. Rep. 36, Neutrino Factory and Muon Collider Collaboration (1999), `http://nfmcc-docdb.fnal.gov/cgi-bin/DocumentDatabase`.

[20] S. Lee, *Accelerator Physics* (World Scientific, 1999).

[21] S. Gilardoni, Tech. Rep. 107, CERN Neutrino Factory Collaboration (2002), `http://slap.web.cern.ch/slap/NuFact/NuFact/NFNotes.html`.

[22] G. Penn and J. Wurtele, Phys. Rev. Lett. **85**, 764 (2000).

[23] G. Penn, Tech. Rep. 71, Neutrino Factory and Muon Collider Collaboration (2000), `http://nfmcc-docdb.fnal.gov/cgi-bin/DocumentDatabase`.

[24] R. Fernow, Tech. Rep. 244, Neutrino Factory and Muon Collider Collaboration (2002), `http://nfmcc-docdb.fnal.gov/cgi-bin/DocumentDatabase`.

[25] C. Wang and K. Kim, Phys. Rev. E **63**, 056502 (2001).

[26] R. Palmer and R. Fernow, `http://pubweb.bnl.gov/users/palmer/www/course`, US Particle Accelertor School, Vanderbilt University.

[27] R.B. Palmer, Tech. Rep. 22, Brookhaven National Laboratory (1998), `http://pubweb.bnl.gov/users/palmer/www/notes/whyalt.ps`.

[28] M. Reiser, *Theory and Design of Charged Particle Beams* (Wiley, 1994).

[29] M.W. Garrett, J. Appl. Phys. **34**, 2567 (1963).

[30] A.M. Clogston and H. Heffner, J. Appl. Phys. **25**, 436 (1954).

[31] G. Caporaso and A. Cole, in *The Physics of Particle Accelerators* (1992), pp. 1615–1712.

[32] R. Fernow, Tech. Rep. 23, Neutrino Factory and Muon Collider Collaboration (1999), `http://nfmcc-docdb.fnal.gov/cgi-bin/DocumentDatabase`.

[33] B. L. Militsyn et al., in *Proceedings of the 2000 European Particle Accelerator Conference* (2000), pp. 1054–1056.

[34] M. Preto and S. Tremaine, Astron. J. **118**, 2532 (1999).

[35] V. Balbekov, Tech. Rep. 190, Neutrino Factory and Muon Collider Collaboration (2001), `http://nfmcc-docdb.fnal.gov/cgi-bin/DocumentDatabase`.

[36] A. Chao and M. Tigner, *Handbook of Accelerator Physics and Engineering* (World Scientific, 1999), page 402.

[37] M. Green, Tech. Rep. 165, Neutrino Factory and Muon Collider Collaboration (2000), `http://nfmcc-docdb.fnal.gov/cgi-bin/DocumentDatabase`.

[38] J.S. Berg *et al.*, Phys. Rev. ST Accel. Beams **9**, 011001 (2006).

[39] J. Monroe *et al.*, Phys. Rev. ST Accel. Beams **4**, 041301 (2001).

[40] S. Ozaki, R. Palmer, M. Zisman, and J. Gallardo, eds., Tech. Rep., BNL-52623 (2001), `http:`

//www.cap.bnl.gov/mumu/studyii/FS2-report.html.

[41] R. Fernow, Tech. Rep. 241, Neutrino Factory and Muon Collider Collaboration (2002), http://nfmcc-docdb.fnal.gov/cgi-bin/DocumentDatabase.